Weiss mean-field approximation for multicomponent stochastic spatially extended systems

Svetlana E. Kurushina and Valerii V. Maximov
Physics Department, Samara State Aerospace University named after S.P. Korolyov, Moskovskoye Shosse 34, 443086 Samara, Russian Federation,
and Mathematics Department, Samara State Transport University, First Bezimyannii Pereulok 18, 443066 Samara, Russian Federation

Yurii M. Romanovskii
Physics Department, Lomonosov Moscow State University, GSP-1, Leninskie Gory, 119991 Moscow, Russian Federation
(Received 3 June 2014; published 26 August 2014)

We develop a mean-field approach for multicomponent stochastic spatially extended systems and use it to obtain a multivariate nonlinear self-consistent Fokker-Planck equation defining the probability density of the state of the system, which describes a well-known model of autocatalytic chemical reaction (brusselator) with spatially correlated multiplicative noise, and to study the evolution of probability density and statistical characteristics of the system in the process of spatial pattern formation. We propose the finite-difference method for the numerical solving of a general class of multivariate nonlinear self-consistent time-dependent Fokker-Planck equations. We illustrate the accuracy and reliability of the method by applying it to an exactly solvable nonlinear Fokker-Planck equation (NFPE) for the Shimizu-Yamada model [Prog. Theor. Phys. **47**, 350 (1972)] and nonlinear Fokker-Planck equation [Desai and Zwanzig, J. Stat. Phys. **19**, 1 (1978)] obtained for a nonlinear stochastic mean-field model introduced by Kometani and Shimizu [J. Stat. Phys. **13**, 473 (1975)]. Taking the problems indicated above as an example, the accuracy of the method is compared with the accuracy of Hermite distributed approximating functional method [Zhang *et al.*, Phys. Rev. E **56**, 1197 (1997)]. Numerical study of the NFPE solutions for a stochastic brusselator shows that in the region of Turing bifurcation several types of solutions exist if noise intensity increases: unimodal solution, transient bimodality, and an interesting solution which involves multiple "repumping" of probability density through bimodality. Additionally, we study the behavior of the order parameter of the system under consideration and show that the second type of solution arises in the supercritical region if noise intensity values are close to the values appropriate for the transition from bimodal stationary probability density for the order parameter to the unimodal one.

DOI: 10.1103/PhysRevE.90.022135 PACS number(s): 05.40.−a, 05.10.−a, 02.70.Bf, 82.40.Ck

I. INTRODUCTION

Mean-field approximation (MFT) is an effective tool for the study of noise-driven dynamics of systems of different nature and noise-induced phenomena [1]. It is successfully applied for the study of noise-induced phase separation in conserved-order-parameter systems [2], the noise-driven mechanism of pattern formation [3], intrinsic noise-induced phase transitions [4], nonequilibrium first-order phase transition induced by additive [5] and multiplicative [6,7] noise, noise-induced reentrant transition in nonlinear chains [8], pure noise-induced nonequilibrium second-order reentrant phase transition [9], and reentrant disorder-order-disorder and order-disorder-order phase transitions with the saddle-point phase diagram structure [10].

In quantum mechanics MFT implies the replacement of a multiparticle interaction Hamiltonian with a single-particle one. Weiss MFT for spatially extended systems implies that the interaction between a certain spatial point and its nearest neighbors occurs through the field, whose value corresponds to the statistically average field at this point. Herewith, a suitable way is used to carry out the discretization of the space of the initial spatially extended system and the Fokker-Planck equation (FPE) for the multivariate probability density function can be written for field values in the points of the obtained regular lattice. The obtained FPE is integrated over the values of the field at all points except the given one. This leads to FPE for the one-dimensional probability distribution density for field values at a given point. In the latter equation the conditional average values of the field at neighboring points are replaced with an average value of the field at a given point [2].

Many real physical, chemical, biological, etc., systems are multicomponent ones and they are modeled by means of partial differential equation systems. However, in [1–10] only single-component spatially extended systems with additive, multiplicative, or both noise types are considered. Therefore, one of the purposes of the present paper is to extend MFT for multicomponent stochastic reaction-diffusion systems which are a specific, but extremely important case of spatially extended systems.

Applying MFT to the study of noise-induced phenomena arising in single-component problems leads to the necessity of numerical solution of a single-site nonlinear self-consistent Fokker-Planck equation (NSCFPE). Various methods are used for the numerical integration of NSCFPE. In [11,12] an elegant and effective method based on Hermite distributed approximating functionals (DAF) is presented. High precision of the solution is achieved at small numbers of grid points. In [13] the finite-difference method based on a K-point Stirling interpolation formula is proposed. In Ref. [14] a finite-difference scheme is used in the differential part and the trapezoid rule in the integral part of NFPE. Finite element [15] and finite-difference methods [15,16], discrete singular convolution algorithm [17], direct quadrature based method of moments [18,19], pseudospectral method [20],

path-integral [21,22] and eigenfunction expansion methods [23,24], and others [25,26] are also used to find numerical solutions of NFPEs.

Despite the variety of existing numerical methods of NFPE solution, only a few of them, for example [12,15], are successfully applied for the integration of multidimensional equations. Therefore, numerical solution of multivariate NSCFPE is still a challenging problem, and the second purpose of the present paper is to propose the numerical method for this problem and to test its accuracy and reliability.

Finally, the third purpose is to apply the mean-field approach proposed and the method developed in Ref. [27] to the research of evolution of probability distribution density and statistical characteristics in the process of spatial pattern formation in the "brusselator" model [28], which incorporates parameter fluctuations, and to compare the results of these approaches.

The rest of this paper is organized as follows. In Sec. II we introduce a generalized mean-field approach developed for multicomponent stochastic reaction-diffusion systems and taking into account the spatial correlation of the external noise. In Sec. III the finite-difference method for numerically solving a general class of multivariate nonlinear self-consistent time-dependent Fokker-Planck equations is presented. The accuracy and reliability of the presented method are demonstrated by applying it to NSCFPE for the Shimizu-Yamada model [29,30] and the Desai-Zwanzig model [31]. The results of comparing the accuracy of the proposed method with the accuracy of the Hermite DAF method [11] are reviewed. A two-dimensional NSCFPE for spatially extended stochastic brusselator is derived in Sec. IV. Different types of this system probability density evolution arising with the noise intensity increase in the Turing bifurcation region are presented. The first- and second-order statistical characteristics of the system under consideration are studied. A FPE for order parameters of the system under study is received. Its stationary solutions for the critical mode and its stationary statistical characteristics are explored. Finally, some conclusions are reported in Sec. V.

II. MEAN-FIELD APPROACH FOR MULTICOMPONENT STOCHASTIC REACTION-DIFFUSION SYSTEMS

The system of stochastic equations of the reaction-diffusion type is one of the mathematical models describing the spatiotemporal dynamics of real multicomponent spatially extended systems under the influence of external fluctuating environment and incorporating internal noises:

$$\frac{\partial x_i}{\partial t} = f_i(x_1,\ldots,x_n) + g_i(x_1,\ldots,x_n)\xi_i(\mathbf{r},t) + \eta_i(\mathbf{r},t) + D_i\nabla^2 x_i, \quad i = 1,\ldots,n. \tag{1}$$

In Eq. (1) x_i are state functions of the system, $f_i(x_1,\ldots,x_n)$ and $g_i(x_1,\ldots,x_n)$ are nonlinear functional dependencies defining the interaction and evolution of components x_i in space and in time, and D_i are diffusion coefficients of components. The additive random Gaussian fields $\eta_i(\mathbf{r},t)$ with zero means and correlation functions $K[\eta_i(\mathbf{r},t),\eta_{i'}(\mathbf{r}',t')] = 2\zeta_i\delta(\mathbf{r}-\mathbf{r}')\delta(t-t')\delta_{ii'}$ model internal white noises, in the presence of which and in the absence of multiplicative noise the system can exhibit equilibrium properties. The intensities of internal noises are measured by parameters ζ_i. Hereafter we use the notation $K[F_1,F_2]$ that is defined by the equality $K[F_1,F_2] = \langle F_1F_2\rangle - \langle F_1\rangle\langle F_2\rangle$ for the correlation function. The multiplicative random fields $\xi_i(\mathbf{r},t)$ model the external noises which disturb the system out of equilibrium. They are also Gaussian [32] with zero means, but it is assumed that they are homogeneous and spatioisotropic and can have a nontrivial spatial structure: $K[\xi_i(\mathbf{r},t),\xi_{i'}(\mathbf{r}',t')] = 2\theta_i\Phi_i(|\mathbf{r}-\mathbf{r}'|)\delta(t-t')\delta_{ii'}$, where $\Phi_i(|\mathbf{r}-\mathbf{r}'|)$ are spatial correlation functions of external noises and θ_i are their intensities. Further, to be definite, we use exponential spatial correlation functions: $\Phi_i(|\mathbf{r}-\mathbf{r}'|) = \exp[-k_{fi}(|\mathbf{r}-\mathbf{r}'|)]$. Parameters k_{fi} characterize the correlation lengths r_{fi} of noises: $r_{fi} = 1/k_{fi}$.

In Ref. [2] the main aspects of MFT in application to nonconserved systems with order parameter (model A in terms of literature of critical phenomena) are outlined.

We carry out the discretization of continuous d-dimensional space of the system (1) and obtain a regular d-dimensional lattice with the mesh size Δr and lattice points, the location of which will be characterized by vectors $\mathbf{r}_l, l = 1,\ldots,p$. Thus, regardless of the dimensionality of the lattice, each lattice point will correspond to only one index. We assume that the interaction takes place only between the nearest neighbors, which allows us to approximate the Laplace operator with a finite-difference expression with a second-order difference. As a result of the discretization the system (1) is replaced with the system $n \times p$ of ordinary differential equations,

$$\frac{dx_{il}}{dt} = F_{il}(t), i = 1,\ldots,n; \quad l = 1,\ldots,p,$$
$$F_{il}(t) = f_{il} + g_{il}\xi_{il}(t) + \eta_{il}(t) + \frac{D_i}{2d(\Delta r)^2}\sum_{l'}\Lambda_{ll'}x_{il'}. \tag{2}$$

In Eqs. (2) the following notations are introduced: $f_{il} = f_i(x_{1l},\ldots,x_{nl})$, $g_{il} = g_i(x_{1l},\ldots,x_{nl})$. $\sum_{l'}\Lambda_{ll'}$ is the discrete analog of the Laplace operator [2]: $\sum_{l'}\Lambda_{ll'} = \sum_{l'}(\delta_{nn(l),l'} - 2d\delta_{l,l'})$, where $nn(l)$ is a set of indexes of all sites which are the nearest neighbors of the site with index l. The discrete noises $\eta_{il}(t)$, $\xi_{il}(t)$ have the correlation functions

$$K[\eta_{il}(t),\eta_{i'l'}(t')] = 2\zeta_i\frac{\delta_{ll'}}{(\Delta r)^d}\delta(t-t')\delta_{ii'} \quad \text{and}$$
$$K[\xi_{il}(t),\xi_{i'l'}(t')] = 2\theta_i\Phi_{i,|l-l'|}\delta(t-t')\delta_{ii'}. \tag{3}$$

Here we have incorporated the fact that the continuum δ function $\delta(\mathbf{r}-\mathbf{r}')$ has been replaced in the usual way with a ratio that contains the Kronecker δ and the lattice spacing $\delta_{ll'}/(\Delta r)^d$, and $\Phi_{i,|l-l'|}$ is convenient discretization of function $\Phi_i(|\mathbf{r}-\mathbf{r}'|)$. The values of $\Phi_{i,0}$ required further can be computed numerically [33].

The Fokker-Planck equation corresponding to Eqs. (2) in the Stratonovich interpretation [34] for multivariate probability density $\tilde{w}(x_{11},\ldots,x_{1l},\ldots,x_{1p},\ldots,x_{n1},\ldots,$

$x_{nl},\ldots,x_{np};t)=\tilde{w}(\{x_1,\ldots,x_n\};t)$ has the form

$$\frac{\partial\tilde{w}(\{x_1,\ldots,x_n\};t)}{\partial t}=-\sum_{i=1}^{n}\sum_{l'=1}^{p}\frac{\partial}{\partial x_{il'}}\left(\left\{\langle F_{il'}(t)\rangle+\sum_{j=1}^{n}\sum_{m=1}^{p}\int_{-\infty}^{0}K\left[\frac{\partial F_{il'}(t)}{\partial x_{jm}},F_{jm}(\tau)\right]d\tau\right\}\tilde{w}\right)$$
$$+\sum_{i,j=1}^{n}\sum_{m,l'=1}^{p}\frac{\partial^2}{\partial x_{il'}x_{jm}}\left(\left\{\int_{-\infty}^{0}K[F_{il'}(t),F_{jm}(\tau)]d\tau\right\}\tilde{w}\right) \tag{4}$$

for all lattice points.

Considering Eqs. (2) the correlators included in Eq. (4) are easily computed,

$$K\left[\frac{\partial F_{il'}(t)}{\partial x_{jm}},F_{jm}(\tau)\right]=\frac{\partial g_{il'}}{\partial x_{jm}}g_{jm}K[\xi_{il'}(t),\xi_{jm}(\tau)]\delta_{ij}\delta_{ml'},\quad m=l,nn(l),$$
$$K[F_{il'}(t),F_{jm}(\tau)]=\{g_{il'}g_{jm}K[\xi_{il'}(t),\xi_{jm}(\tau)]+K[\eta_{il'}(t),\eta_{jm}(\tau)]\}\delta_{ij}\delta_{ml'},\quad m=l,nn(l). \tag{5}$$

After the substitution of correlators (5) and (3) into Eq. (4) and some simple transformations the equation for multivariate probability density $\tilde{w}(\{x_1,\ldots,x_n\};t)$ will appear as

$$\frac{\partial\tilde{w}(\{x_1,\ldots,x_n\};t)}{\partial t}=-\sum_{i=1}^{n}\sum_{l'=1}^{p}\frac{\partial}{\partial x_{il'}}\left[f_{il'}+\frac{D_i}{2d(\Delta r)^2}\left(\sum_{m=nn(l')}x_{im}-2dx_{il'}\right)-\sum_{m=l',nn(l')}\left(\zeta_i\frac{\partial}{\partial x_{im}}-\theta_i g_{il'}\Phi_{i,|l'-m|}\frac{\partial}{\partial x_{im}}g_{im}\right)\right]\tilde{w}. \tag{6}$$

We choose one site with index l. In order to obtain multivariate probability density $w(x_{1l},\ldots,x_{il},\ldots,x_{nl};t)=w(\{x\};t)$ for a single site it is necessary to integrate $\tilde{w}(x_{11},\ldots,x_{1l},\ldots,x_{1p},\ldots,x_{n1},\ldots,x_{nl},\ldots,x_{np};t)$ over all the variables except $x_{1l},\ldots,x_{il},\ldots,x_{nl}$:

$$w(x_{1l},\ldots,x_{il},\ldots,x_{nl};t)=\int\tilde{w}(x_{11},\ldots,x_{1l},\ldots,x_{1p},\ldots,x_{n1},\ldots,x_{nl},\ldots,x_{np};t)\left[\prod_{k\neq l}dx_{1k}\cdots dx_{ik}\cdots dx_{nk}\right].$$

We use the property of probability density to vanish at the infinity: $\tilde{w}(\{x_1,\ldots,x_n\};t)\to 0$ if $x_{il}\to\pm\infty, i=1,\ldots,n; l=1,\ldots,p$. Then

$$\int\frac{\partial}{\partial x_{im}}(g_{im}\tilde{w})\left[\prod_{k\neq l}dx_{1k}\cdots dx_{ik}\cdots dx_{nk}\right]=\begin{cases}0, & m\neq l,\\ \frac{\partial}{\partial x_{il}}[g_{il}w(\{x\};t)], & m=l.\end{cases} \tag{7}$$

According to the definition of conditional probability, we can write

$$\int x_{im}\tilde{w}\left[\prod_{k\neq l}dx_{1k}\cdots dx_{ik}\cdots dx_{nk}\right]=\int x_{im}w(x_{1l},\ldots,x_{im},x_{il},\ldots,x_{nl};t)dx_{im}$$
$$=\left[\int x_{im}w(x_{im}|x_{1l},\ldots,x_{il},\ldots,x_{nl};t)dx_{im}\right]w(x_{1l},\ldots,x_{il},\ldots,x_{nl};t)$$
$$=w(\{x\};t)E(x_{im}|x_{1l},\ldots,x_{il},\ldots,x_{nl};t). \tag{8}$$

Here $E(x_{im}|x_{1l},\ldots,x_{il},\ldots,x_{nl};t)$ are nearest-neighbor conditional averages.

Finally, taking into account Eqs. (7) and (8), we get

$$\frac{\partial w(\{x\};t)}{\partial t}=-\sum_{i=1}^{n}\frac{\partial}{\partial x_{il}}\left\{f_{il}+\frac{D_i}{2d(\Delta r)^2}\left[\sum_{m=nn(l)}E(x_{im}|x_{1l},\ldots,x_{il},\ldots,x_{nl};t)-2dx_{il}\right]-\zeta_i\frac{\partial}{\partial x_{il}}-\theta_i\Phi_{i,0}g_{il}\frac{\partial}{\partial x_{il}}g_{il}\right\}w \tag{9}$$

for single-point multivariate probability density.

Taking into account that x_{il} are linked by Eqs. (2) let us assume that the MFT is to imply that the conditional average $E(x_{im}|x_{1l},\ldots,x_{il},\ldots,x_{nl};t)$ in Eq. (9) can be replaced with the conditional average $E(x_{il}|x_{1l},\ldots,x_{i-1l},x_{i+1l},\ldots,x_{nl};t)$:

$$E(x_{im}|x_{1l},\ldots,x_{il},\ldots,x_{nl};t)=E(x_{il}|x_{1l},\ldots,x_{i-1l},x_{i+1l},\ldots,x_{nl};t), \tag{10}$$

$$E(x_{il}|x_{1l},\ldots,x_{i-1l},x_{i+1l},\ldots,x_{nl};t)=\int_{-\infty}^{+\infty}x_{il}w(x_{il}|x_{1l},\ldots,x_{i-1l},x_{i+1l},\ldots,x_{nl};t)dx_{il},$$

$$w(x_{il}|x_{1l},\ldots,x_{i-1l},x_{i+1l},\ldots,x_{nl};t)=\frac{w(\{x\};t)}{\int_{-\infty}^{+\infty}w(x_{1l},\ldots,x_{il},\ldots,x_{nl};t)dx_{il}}. \tag{11}$$

In this approximation the exact FPE (9) is transformed into an approximate

$$\frac{\partial w([x];t)}{\partial t} = \sum_{i=1}^{n} \frac{\partial}{\partial x_{il}} \left[C^{i}_{\text{drift}}([x],w,t)w + \frac{\partial}{\partial x_{il}} \left(C^{i}_{\text{diff}}([x],t)w \right) \right], \quad (12)$$

where $C^{i}_{\text{drift}}([x],w,t) = -f_{il} - \frac{D_i}{(\Delta r)^2}[E(x_{il}|x_{1l},\ldots,x_{i-1l}, x_{i+1l},\ldots,x_{nl};t) - x_{il}] - \theta_i \Phi_{i,0} g_{il} \frac{\partial g_{il}}{\partial x_{il}}$ are generalized drift coefficients and $C^{i}_{\text{diff}}([x],t) = \zeta_i + \theta_i \Phi_{i,0} g^2_{il}$ are diffusion coefficients. Hereafter the index l is omitted for the simplicity of writing.

Equations (10)–(12) form a self-consistent system for which it is impossible to write a stationary solution even implicitly as opposed to the one-dimensional case. The numerical solution of (10)–(12) is a complicated problem. The next section is devoted to the development of a numerical method for the solution of this problem and testing its accuracy and reliability.

III. NUMERICAL METHOD FOR THE MULTIVARIATE NONLINEAR SELF-CONSISTENT FOKKER-PLANCK EQUATION

A. Finite-difference method

A multivariate NSCFPE (12) can be presented as

$$\frac{\partial w}{\partial t} = \sum_{\alpha=1}^{n} \frac{\partial}{\partial x_\alpha} \left[k_\alpha(x,t) \frac{\partial w}{\partial x_\alpha} - \rho_\alpha(x,t) w \right] = \sum_{\alpha=1}^{n} L_\alpha w,\ x = (x_1,\ldots,x_n),\ \alpha = 1,\ldots,n, \quad (13)$$

where $k_\alpha(x,t) = C^{\alpha}_{\text{diff}}([x],t), k_\alpha(x,t) > 0, \rho_\alpha(x,t) = C^{\alpha}_{\text{drift}}([x],w,t) + 2\theta_\alpha \Phi_{\alpha,0} g_\alpha \frac{\partial g_\alpha}{\partial x_\alpha}$.

Here $x = (x_1,\ldots,x_n)$ belong to the region G. The functions $\rho_\alpha(x,t)$ implicitly depend on w [see Eq. (11)].

Let us choose natural boundary conditions (BCs) for the probability density,

$$w(x,t) \to 0 \ \text{ if } \ x_\alpha \to \pm\infty, \quad (14)$$

and the initial condition (IC)

$$w(x,0) = w_0(x). \quad (15)$$

Let us transform the operators L_α to the form

$$L_\alpha = \frac{\partial}{\partial x_\alpha} \left[\frac{k_\alpha}{q_\alpha} \frac{\partial}{\partial x_\alpha} (q_\alpha w) \right], \quad q_\alpha = \exp \int \frac{\rho_\alpha}{k_\alpha} dx_\alpha. \quad (16)$$

The functions q_α from (16) obtained by integrating over x_α include the conditional average $E(x_\alpha|x_1,\ldots,x_{\alpha-1},x_{\alpha+1},\ldots,x_n;t)$ that represents the function of the variables $x_1,\ldots,x_{\alpha-1},x_{\alpha+1},\ldots,x_n$ except x_α. Finding q_α, therefore, does not present a problem. If $\int (\rho_\alpha/k_\alpha) dx_\alpha$ cannot be integrated precisely, one can use approximative methods, for example, the trapezoid rule.

For the problem (13)–(15) we choose a rectangular spatial mesh $\omega_h = (\{x_i\} = \{i_1 h_1,\ldots,i_\alpha h_\alpha,\ldots,i_n h_n\} \in G)$, where $i_1,\ldots,i_n$ $(i_\alpha = 0,1,\ldots,N_\alpha)$ and $h_1,\ldots,h_n$ are the indices of the mesh points and the steps, respectively, and ω_τ is a time mesh with a step τ over the interval $0 \leqslant t \leqslant T$. For the mesh functions given on $\omega_h \times \omega_\tau$ we use the following notations: $y = y^{j+\alpha/n} = y(x_i,t_{j+\alpha/n})$, $y_{\bar{x}_\alpha} = [y(x_{1,i_1},\ldots,x_{\alpha,i_\alpha},\ldots,x_{n,i_n},t) - y(x_{1,i_1},\ldots,x_{\alpha,i_\alpha-1},\ldots,x_{n,i_n},t)]/h_\alpha$ is the left-side difference derivative at the point $x_{1,i_1},\ldots,x_{\alpha,i_\alpha},\ldots,x_{n,i_n}$, and $y_{x_\alpha} = [y(x_{1,i_1},\ldots,x_{\alpha,i_\alpha+1},\ldots,x_{n,i_n},t) - y(x_{1,i_1},\ldots,x_{\alpha,i_\alpha},\ldots,x_{n,i_n},t)]/h_\alpha$ is the right-side difference derivative at the point $x_{1,i_1},\ldots,x_{\alpha,i_\alpha},\ldots,x_{n,i_n}$.

Applying the finite-volume method [35] we associate L_α to difference analogs [36],

$$\Lambda_\alpha y = \left[a_\alpha (q_\alpha y)_{\bar{x}_\alpha} \right]_{x_\alpha}, \quad (17)$$

where $a_{\alpha,i} = \left[\int_{x_{\alpha,i_\alpha-1}}^{x_{\alpha,i_\alpha}} \frac{q_\alpha}{k_\alpha} dx_\alpha \right]^{-1}$.

A locally one-dimensional scheme for the problem (13)–(15) will take the form

$$\frac{y^{j+\alpha/n} - y^{j+(\alpha-1)/n}}{\tau} - \Lambda_\alpha y = 0, \quad y^0 = w_0. \quad (18)$$

It is shown in Refs. [36,37] that scheme (18) is unconditionally stable in the Banach space with the norm $\|y\| = \sum_{i_1}^{N_1-1} \cdots \sum_{i_n}^{N_n-1} |y(x_{1,i_1},\ldots,x_{\alpha,i_\alpha},\ldots,x_{n,i_n})| h_1 \cdots h_n$ and has the accuracy $O(\tau + \sum_\alpha h_\alpha^2)$.

Depending on the sign of the function $\rho_\alpha(x,t)$, we can use the appropriate variant of a tridiagonal matrix algorithm or any other method of solving systems of linear algebraic equations. The integrals (11) are easily calculated using the Simpson's rule from the preceding layer.

B. Accuracy, reliability, and limitations

To demonstrate the accuracy and reliability of the results obtained with the help of the finite-difference scheme (18) and to find out its limitations, we apply (18) to the exactly solvable NFPE for the Shimizu-Yamada model [29,30] and the NFPE [31] obtained for the nonlinear stochastic mean-field model introduced by Kometani and Shimizu [38]. The accuracy of the method is compared with the accuracy of Hermite DAF method [11] taking the problems indicated above as an example.

The NSCFPE for Shimizu-Yamada model has the form

$$\frac{\partial f(x,t)}{\partial t} = \frac{\partial \{[\omega x + \theta Ex(t)] f(x,t)\}}{\partial x} + D \frac{\partial^2 f(x,t)}{\partial x^2}, \quad (19)$$

where $Ex(t) = \int_{-\infty}^{+\infty} x f(x,t) dx$ is mathematical expectation, ω, θ, and D are constants. With the initial spatial distribution in the form of the Dirac δ function $f(x,0) = \delta(x - x_0)$ the exact solution of the problem (19) takes the form (Fig. 1)

$$f(x,t) = \frac{1}{\sqrt{2\pi\sigma(t)}} \exp\left\{ -\frac{[x - Ex(t)]^2}{2\sigma(t)} \right\}, \quad (20)$$

where $Ex(t) = x_0 e^{-(\omega+\theta)t}$, $\sigma(t) = \frac{D}{\omega}(1 - e^{-2\omega t})$.

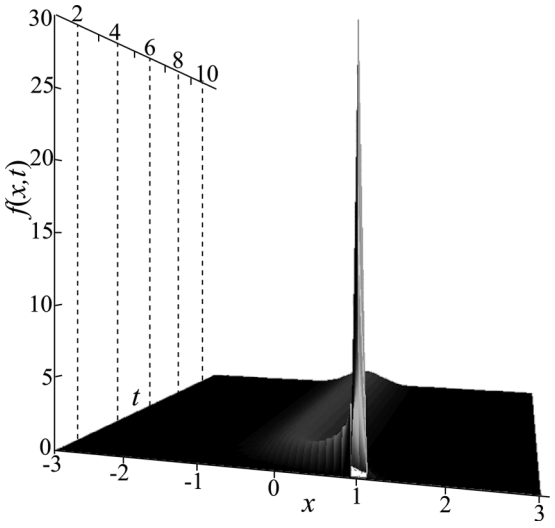

FIG. 1. Analytical solution (20) for the problem (19). Hereafter the parameters $\omega = 1, \theta = 1, D = 0.1$, and $x_0 = 1$ are chosen for the problem (19).

The accuracy and reliability of the scheme (18) was determined by the relative error

$$\varepsilon(t) = \frac{\{Ex^2(t) - [Ex(t)]^2\}|_{\text{Num}}}{\sigma(t)} - 1. \qquad (21)$$

The expression $\{Ex^2(t) - [Ex(t)]^2\}|_{\text{Num}}$ is the second moment obtained in solving (19) by various numerical methods. Additional control was accomplished by checking the fulfillment of the condition of probability density normalization per unit $1(t) = \int_{-\infty}^{+\infty} f(x,t)dx$ at each time step. The condition was also used as the criterion of the correct choice of the integration region size governing the observation of boundary conditions (14).

Figures 2 and 3 compare the plots of the decimal logarithm of the relative error $\log_{10}|\varepsilon(t)|$ and the decimal logarithm of the deviation of probability density normalization from unit $\log_{10}|1 - 1(t)|$. Figures 4(a), 4(b), 5(a), and 5(b) demonstrate numerical solutions of Eq. (19) obtained on the basis of the scheme (18) and the method based on DAF and the decimal logarithm of module of absolute error $f(x,t) - f(x,t)_{\text{Eq.(20)}}$ defining the deviation of numerical solution from the analytical

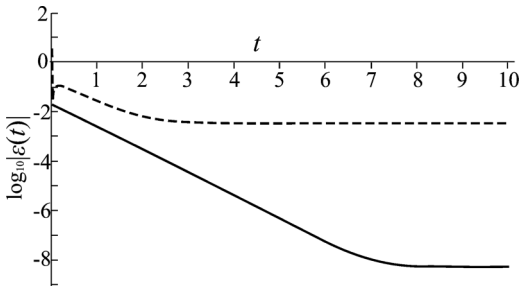

FIG. 2. Dependencies of the decimal logarithm of the relative error $\log_{10}|\varepsilon(t)|$ (21) on time. The dashed line is the DAF-based method [11]; the solid line is the finite-difference method (18).

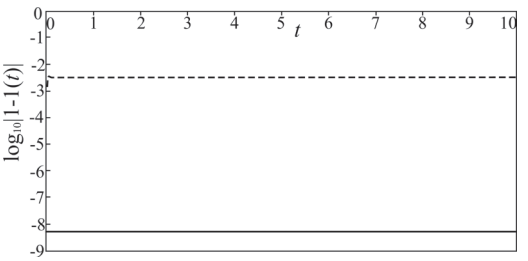

FIG. 3. Dependencies of logarithm of the probability density normalization deviation $\log_{10}|1 - 1(t)|$ from unity on time. The dashed line is the DAF-based method; the solid line is the finite-difference method (18).

one Eq. (20). Figure 6 shows the dependencies $f(x)$ for $t = 0.01$ for the analytical solution and the solutions obtained by methods (18) and DAF. The appropriate dependencies are obtained for the parameters recommended (giving the least error) in [11] for the DAF-based method in the proper order of

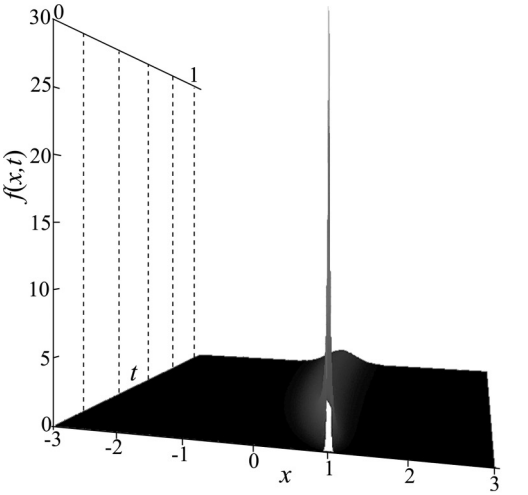

(a)

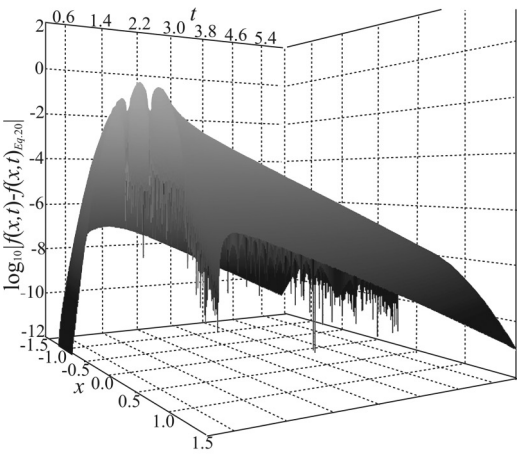

(b)

FIG. 4. Surfaces $f(x,t)$ (a) and $\log_{10}|f(x,t) - f(x,t)_{\text{Eq.(20)}}|$ (b) obtained as a result of the numerical solution (19) by the method (18).

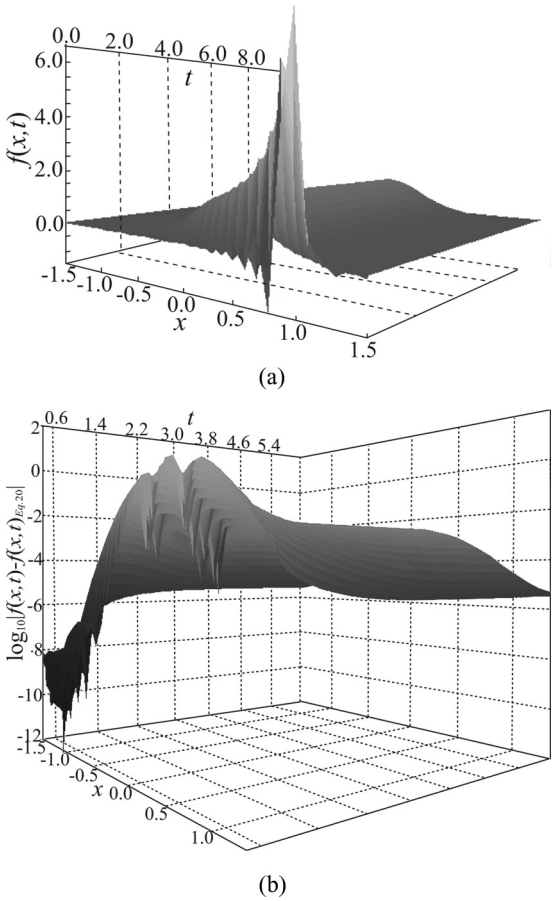

FIG. 5. Surfaces $f(x,t)$ (a) and $\log_{10}|f(x,t) - f(x,t)_{\text{Eq.(20)}}|$ (b) obtained as a result of the numerical solution (19) by the DAF-based method.

time approximation $[O(\tau)]$, the same as in scheme (18). The solution by the scheme (18) is obtained for $h_1 = \tau = 0.001$.

It can be seen from the plots presented in Figs. 2, 4(b), and 5(b) that in the first order of approximation over time the accuracy of the solution obtained by using scheme (18) is higher, especially when steady-state values are reached and time moments are close to the initial one. Figure 3 shows that the values $\log_{10}|1 - 1(t)|$ obtained by the DAF-based method have order 10^{-2}, which means some violation of the normalization condition. On the contrary, scheme (18) conserves asymptotically (at large times) the condition of normalization of probability density per unit with precision of order 10^{-8}. The analysis of Figs. 1, 4, 5, and 6 shows that scheme (18) provides the positive definiteness of probability density values at time moments close to the initial one, where the solution is close to discontinuity, and a higher precision of the solution.

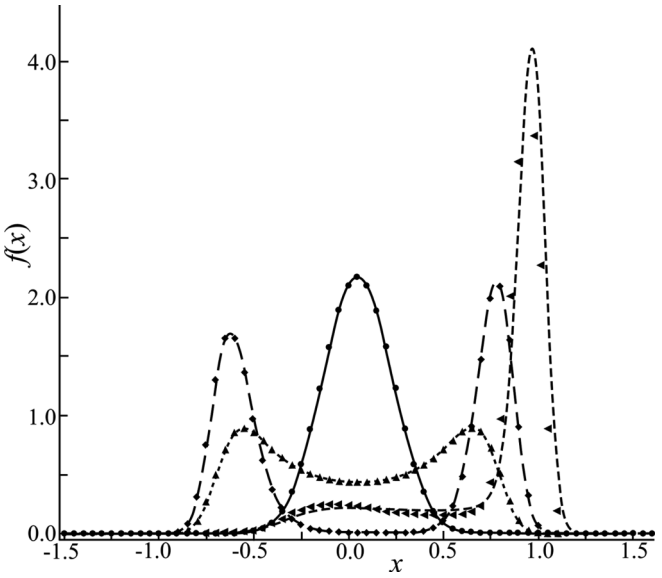

FIG. 7. Distributions $f(x)$ at time moments $t = 1$, 4, 72, 105.5 obtained on the basis of scheme (18) (lines) and on the basis of the DAF method (separate symbols). $t = 1$, solid line, circles; $t = 4$, dotted line, triangles; $t = 72$, line with long dashes, squares; $t = 105.5$, dashed line, rotated triangles. Hereinafter, the parameters $\theta = 0.5$, $D = 0.01$, and $x_0 = 10^{-4}$ are chosen for the problem (22).

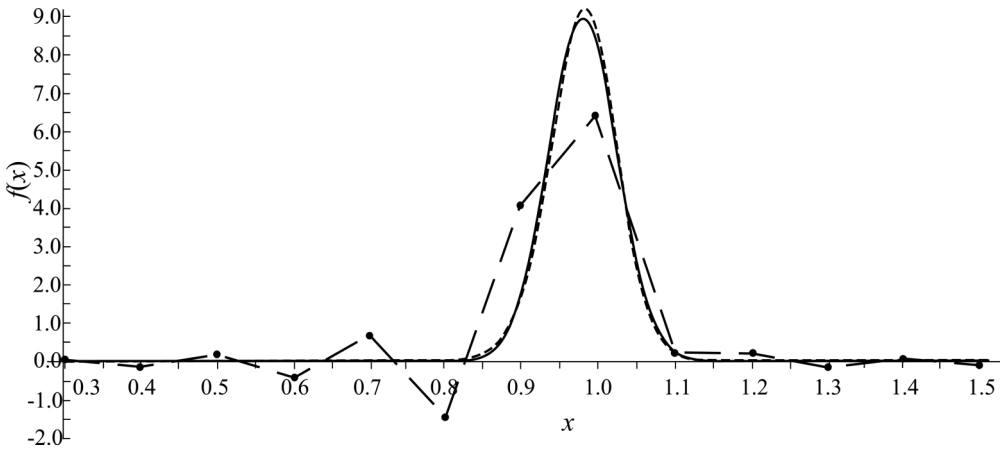

FIG. 6. The dependence of probability density $f(x)$ at $t = 0.01$. The solid line is the analytical solution (20), the dashed line is the solution obtained by method (18), and the line with a long dashes is the DAF-based method [11].

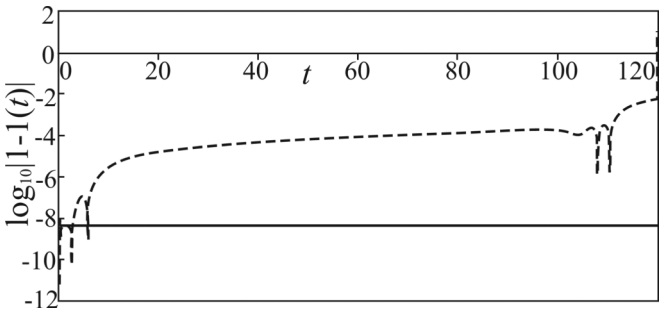

FIG. 8. Dependencies of the logarithm of normalization deviation from unit on time for the problem (22). The dashed line is the DAF-based method [11]; the solid line is the finite-difference method (18).

The second problem chosen for the examination of scheme (18),

$$\frac{\partial f(x,t)}{\partial t} = \frac{\partial(\{x^3 + (\theta-1)x - \theta E[x(t)]\} f(x,t))}{\partial x} + D\frac{\partial^2 f(x,t)}{\partial x^2}, \quad (22)$$

has a larger computational complexity than problem (19), since long-lived bimodality is observed here at certain parameters, and consequently calculations are to be performed for large times. It imposes an additional requirement—asymptotic stability—on the numerical method.

The problem (22) was solved numerically in Ref. [11] by Hermite DAF method. Below the distributions $f(x)$ at different time moments, the dependencies of normalization $1(t)$ on time, mean $E[x(t)]$, variance $Dx(t) = Ex^2(t) - [Ex(t)]^2$, and the decimal logarithm of relative error $\log_{10}|\varepsilon_{\text{Num}}(t)| = \frac{Dx(t)|_{\text{Eq.(18)}}}{Dx(t)|_{DAF}} - 1$ are presented in Figs. 7–11 for comparison. In the last expression $Dx(t)|_{\text{Eq.(18)}}$ is the variance calculated on the basis of scheme (18), $Dx(t)|_{DAF}$ is the variance calculated on the basis of the DAF-based method. Here the DAF-based method solution is chosen as a benchmark for comparison.

It can be seen from Fig. 7 that the difference between numerical solutions begins to appear at times of the order of 105.5. Figure 8 gives the explanation for this. It follows from it that significant violation of the normalization condition arises at the same time. Evidently, insignificant differences in dependencies of means $Ex(t)$ and variances $Dx(t)$ (see Figs. 9 and 10) and the increase of relative error (see Fig. 11) are associated with it.

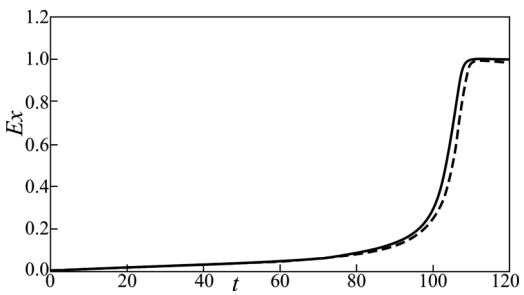

FIG. 9. Expectation $Ex(t)$ vs time. The dashed line is the DAF-based method [11]; the solid line is the finite-difference method (18).

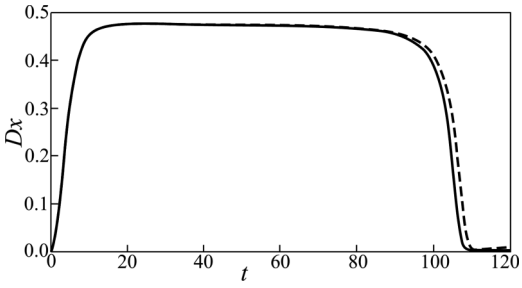

FIG. 10. Variance $Dx(t)$ vs time. The dashed line is the DAF-based method [11]; the solid line is the finite-difference method (18).

Thus, the DAF-based method limitations connected with the violation of probability density normalization condition manifest themselves stronger in the problems with large computational complexity. That is why its stability and the reliability of solution fail at large times. Also, this method violates locally the positive definiteness of solutions required for the fulfillment of the standard properties of the probability density.

Method (18) is free from the above features. The necessity of choosing a sufficiently dense uniform mesh can be classified as a limitation of scheme (18). However, this can be avoided by choosing a mesh with a variable space step. It is possible to construct an unconditionally stable homogeneous conservative finite-difference scheme for problem (13)–(15) on a nonuniform mesh using Refs. [39,40].

IV. SPATIALLY EXTENDED STOCHASTIC BRUSSELATOR

A. Mean-field result

Let us apply the method developed in Sec. III to the study of probability density of the system describing the well-known model of autocatalytic chemical reaction (brusselator [28]) with spatially correlated multiplicative noise. Simultaneously, let us study the variance of some statistical first- and second-order characteristics of the system by increasing the intensity of the external noise. In this paper the range of parameters at which the Turing bifurcation arises in a deterministic system is considered.

Brusselator is a model of a simple autocatalytic chemical reaction having a trimolecular step [28]. The concentrations of the initial and final products in this reaction are maintained constant. The influence of external fluctuating environment

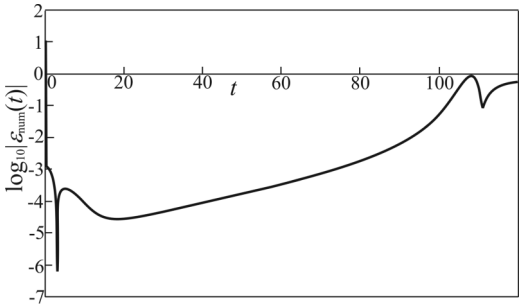

FIG. 11. Decimal logarithm of relative error $\log_{10}|\varepsilon_{\text{Num}}(t)|$ vs time for the problem (22).

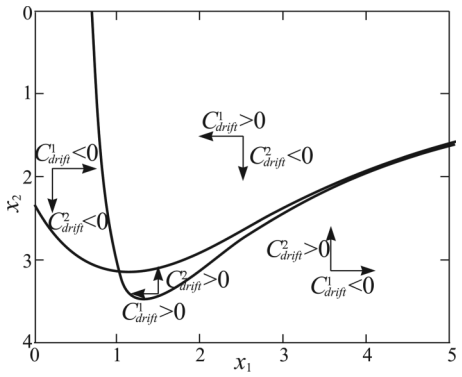

FIG. 12. Probability density (24) drift directions on the plane (x_1,x_2). The solid lines are the boundary of the regions of different drift directions, the regions defined by equations $C^{1,2}_{\text{drift}}(x_1,x_2,w,t) = 0$. Parameters are $A = 3$, $B = 7$, $\theta_1 = \theta_2 = 0.1$, $D_1 = 1$, $D_2 = 5$, $E(x_1|x_2,t) = A, E(x_2|x_1,t) = B/A$, $\Phi_{1,0} = \Phi_{2,0} = 1$.

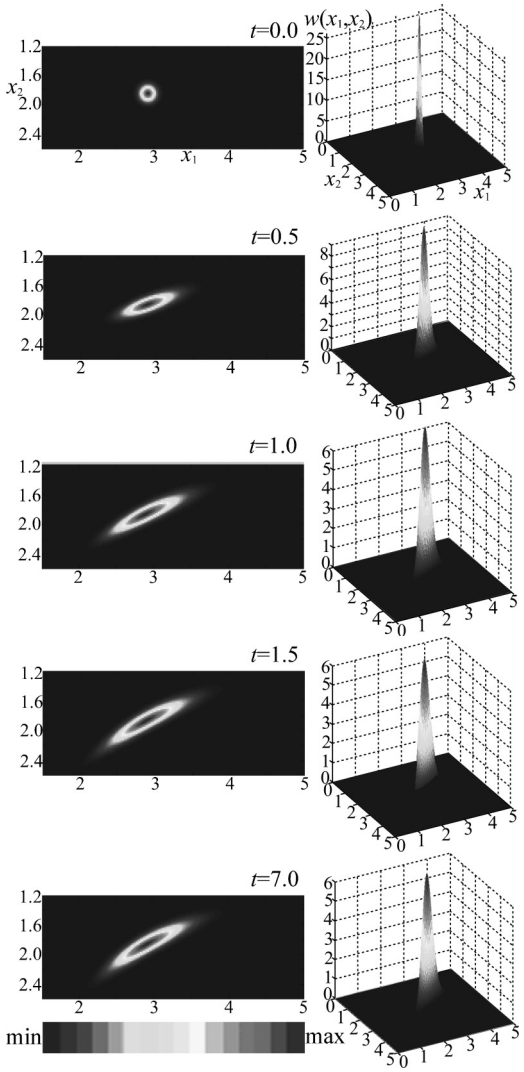

FIG. 13. The evolution of probability density (24) for the model (23). Unimodal distribution (top view in the left-hand side). The color gradient presented in the figure visualizes the change from minimum to maximum. The model parameters are $B = 5.5$, $\theta_1 = \theta_2 = 0.005$. The time moment $t = 7$ corresponds to the stationary state.

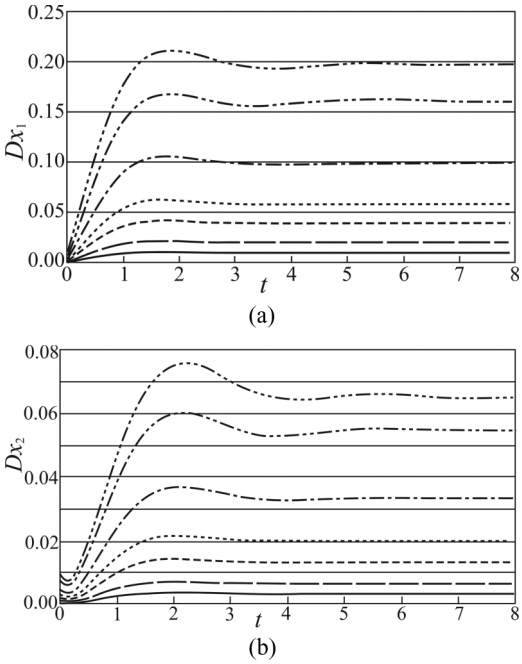

FIG. 14. The dependencies of variance Dx of concentration on time with increasing noise intensity: (a) first product, (b) second product. Solid lines, $\theta_1 = \theta_2 = \theta = 0.0005$; long-dashed lines, $\theta = 0.001$; dashed lines, $\theta = 0.002$; dotted lines, $\theta = 0.003$; dash-dotted lines, $\theta = 0.005$; dash-dot-doted lines, $\theta = 0.008$; the three-dots-dashed line, $\theta = 0.01$. $B = 5.5$.

can lead to the fact that concentrations of the initial and final products become random functions. This leads to the necessity of including noise into the kinetic equations of a deterministic model. Let us assume that the concentration of the initial product B_{in} is most affected by external random environment. Then kinetic equations of the reaction under consideration have the form

$$\begin{aligned}\frac{\partial x_1}{\partial t} &= A + x_1^2 x_2 - [B + 1 + \xi_1(\mathbf{r},t)]x_1 + D_1\nabla^2 x_1,\\ \frac{\partial x_2}{\partial t} &= -x_1^2 x_2 + [B + \xi_2(\mathbf{r},t)]x_1 + D_2\nabla^2 x_2,\end{aligned} \tag{23}$$

where x_1 and x_2 are concentrations of intermediate components, D_1 and D_2 are their diffusion coefficients, and A and B_{in} are concentrations of initial products with $B_{in} = B + \xi_i(\mathbf{r},t)$. Parameter B is the spatiotemporal average of the initial product concentration B_{in}. The decrease in concentration x_1 is due to the two decays: with the formation of one of the final products and with the formation of an intermediate product x_2 and the second final product. These decays have different chemical reaction rates which are affected by external noises in different ways. It is taken into account by including different uncorrelated fields $\xi_i(\mathbf{r},t)$ into Eqs. (23). Statistical properties of the fields $\xi_i(\mathbf{r},t)$ are described in Sec. I.

The system of Eqs. (23) is a specific case of Eq. (1) with $n = 2$. Therefore, multidimensional single-site NSCFPE in the Stratonovitch interpretation can be immediately written for the

model (23) using Eq. (12):

$$\frac{\partial w(x_1,x_2,t)}{\partial t} = \frac{\partial}{\partial x_1}\Big(\big\{-A - x_1^2 x_2 + (B+1+\theta_1\Phi_{1,0})x_1 - D_1[E(x_1|x_2) - x_1]\big\}w + \theta_1\Phi_{1,0}x_1^2\frac{\partial w}{\partial x_1}\Big) + \frac{\partial}{\partial x_2}\Big(\big\{x_1^2x_2 - Bx_1 - D_2[E(x_2|x_1) - x_2]\big\}w + \theta_2\Phi_{2,0}x_1^2\frac{\partial w}{\partial x_2}\Big), \quad (24)$$

$$E(x_1|x_2,t) = \int_{-\infty}^{+\infty} x_1 w(x_1|x_2,t)dx_1,$$

$$E(x_2|x_1,t) = \int_{-\infty}^{+\infty} x_2 w(x_2|x_1,t)dx_2,$$

$$w(x_1|x_2,t) = \frac{w(x_1,x_2,t)}{\int_{-\infty}^{+\infty} w(x_1,x_2,t)dx_1},$$

$$w(x_2|x_1,t) = \frac{w(x_1,x_2,t)}{\int_{-\infty}^{+\infty} w(x_1,x_2,t)dx_2}.$$

Numerical solutions for Eq. (24) are obtained using the finite-difference scheme (18) (see Appendix A). Equation (24) has a greater computational complexity than, for example, the problems (19) and (22). This is related to the fact that, first, the generalized drift coefficients $C^1_{\text{drift}}(x_1,x_2,w,t) = -A - x_1^2x_2 + (B + 1 - \theta_1\Phi_{1,0})x_1 - D_1[E(x_1|x_2) - x_1]$ and $C^2_{\text{drift}}(x_1,x_2,w,t) = x_1^2x_2 - Bx_1 - D_2[E(x_2|x_1) - x_2]$ are nonlinear and of alternating sign. This leads to the fact that regions with the different direction of the probability density drift arise on the plane (x_1,x_2) (see Fig. 12). Moreover, the boundaries of these regions defined by the equations $C^{1,2}_{\text{drift}}(x_1,x_2,w,t) = 0$ are moving since conditional means $E(x_1|x_2,t), E(x_2|x_1,t)$ are time functions. Second, the diffusion coefficients are proportional to x_1^2, which leads to a significant increase of the integration region necessary to satisfy the boundary conditions (14). Third, the problem (24) is two-dimensional and increasing the dimension of the space always leads to an increase of computational complexity.

Figures 13, 17, 21, and 22 present characteristic types of solutions (24) obtained at different values of the parameters of the problem and the noise intensity. The initial distribution is Gaussian with variances θ_1 and θ_2, and expectations equal to stationary values of x_{10} and x_{20} in the absence of noise (see Appendix A). The following parameters for numerical integration (24) remain constant in our calculations: $A = 3$, $D_1 = 1$, $D_2 = 5$, $\Phi_{1,0} = \Phi_{2,0} = 1$. The other parameters are indicated under the figures. The critical value of parameter B is 5.4833 in a deterministic case at given A, D_1, and D_2.

Figure 13 demonstrates the evolution of probability density $w(x_1,x_2,t)$ in the vicinity of the deterministic bifurcation point and small noise intensity. It can be seen from this figure that the symmetry of initial distribution is violated in the evolution process. The probability density distribution remains unimodal throughout the time until the stationary state is reached. Hence, the state of the system (23) is ordered, despite the noise.

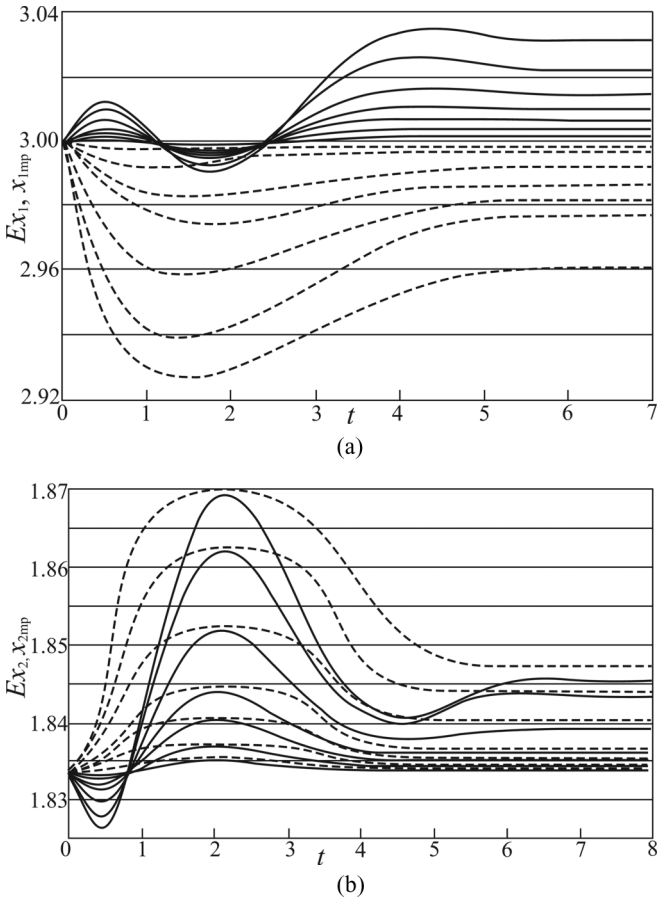

FIG. 15. The dependencies of mean Ex (solid lines) and most probable x_{mp} (dashed lines) values on time in the case of increasing noise intensity: (a) first product, (b) second product. $B = 5.5$. θ_1,θ_2 are as in Fig. 14. The greater the noise intensity, the greater is the deviation of values Ex and x_{mp} from the stationary values of x_{10} and x_{20} ($t = 0$).

Figure 14 shows the appropriate dependencies of variance of concentrations x_1 and x_2 on time if noise intensity increases. It can be seen that the greater external noise intensity, the faster the variance increases and the greater is its value in the

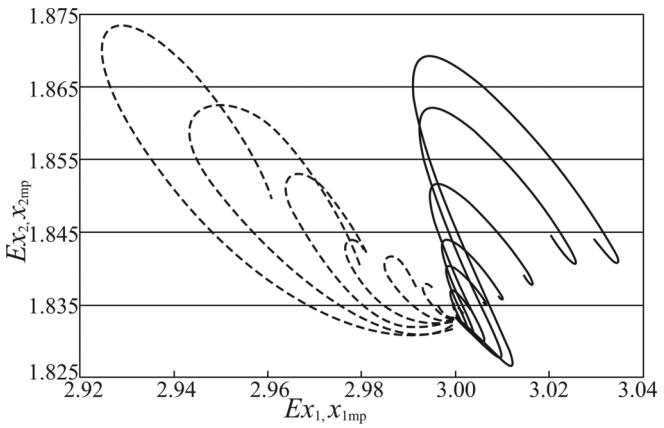

FIG. 16. Changes of the mean Ex (solid lines) and most probable x_{mp} (dashed lines) values x_1 and x_2 in case of increasing noise intensity for unimodal distribution. $B = 5.5$. θ_1,θ_2 are as in Fig. 14. The greater the noise intensity, the greater is the size of the wreath of the curve.

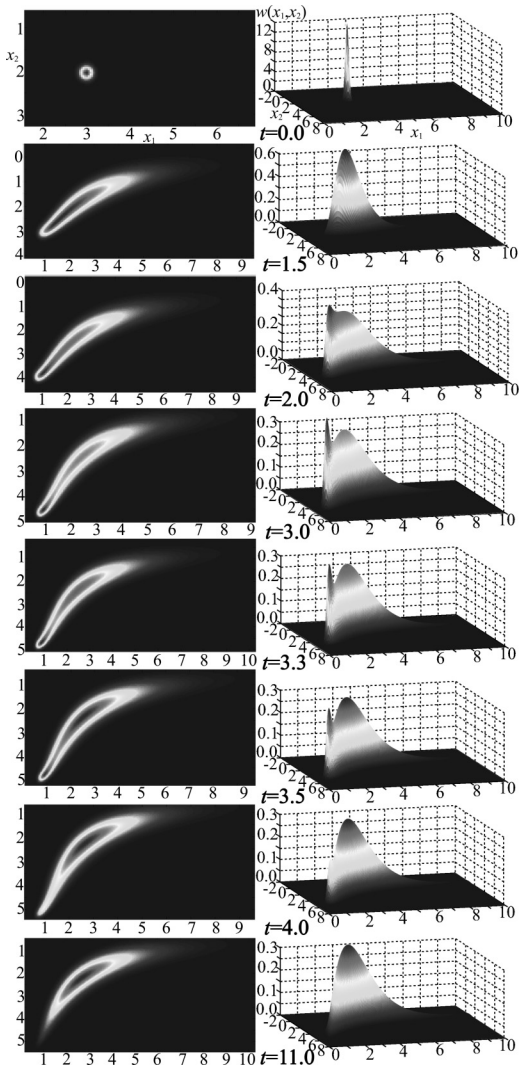

FIG. 17. The evolution of probability density (24) for the model (23). Transient bimodality is observed in the time interval $t \in [1.5,4]$. Model parameters are $B = 6$, $\theta_1 = \theta_2 = 0.09$. The time moment $t = 11$ corresponds to the setting of the stationary state.

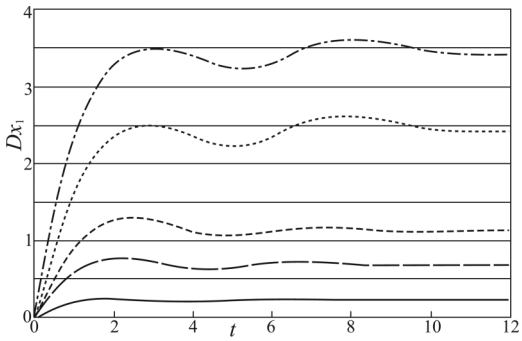

FIG. 18. Dependencies of variance Dx_1 of concentration x_1 on time with increasing noise intensity. Solid line, $\theta_1 = \theta_2 = \theta = 0.01$; long-dashed line, $\theta = 0.03$; dashed line, $\theta = 0.05$; dotted line, $\theta = 0.09$; dash-dotted line, $\theta = 0.12$. $B = 6$.

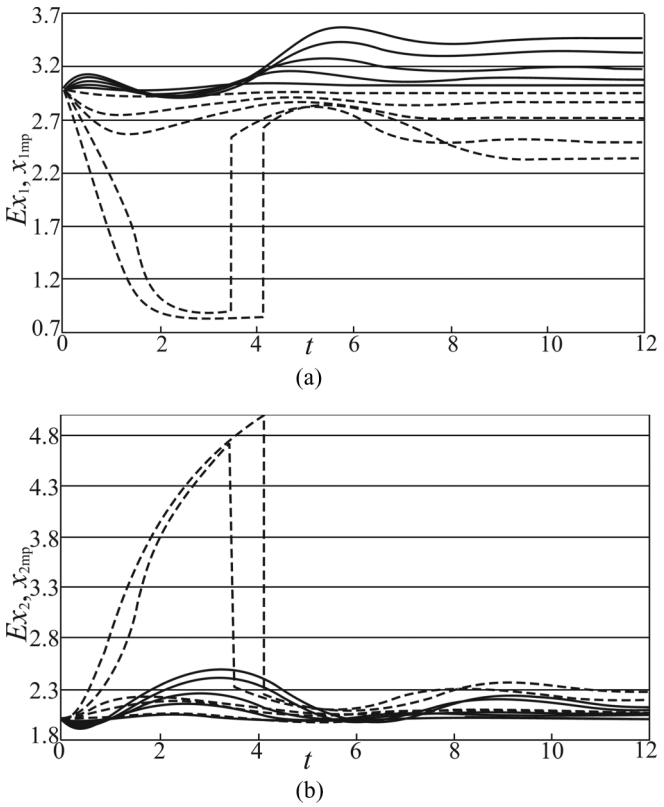

FIG. 19. The dependencies of mean Ex (solid lines) and most probable x_{mp} (dashed lines) values on time with increasing noise intensity: (a) first product, (b) second product. $B = 6$. θ_1,θ_2 are as in Fig. 14. The greater the noise intensity, the greater the deviation of values Ex and x_{mp} from the stationary values of x_{10} and x_{20}. The most probable jump (discontinuity of the first kind) corresponds to the disappearance of bimodality.

stationary state. Figure 15 demonstrates the dependencies of the mean and most probable values on time with different noise intensities. The increase of noise intensity leads to the increase of difference between the mean and the appropriate most

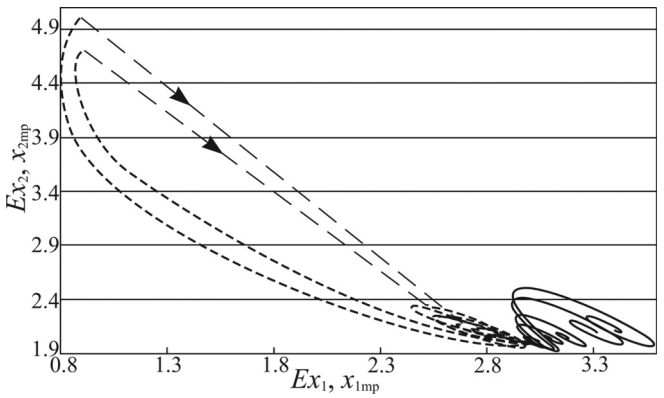

FIG. 20. Changes of the mean Ex (solid lines) and the most probable x_{mp} (dashed lines) values x_1 and x_2 in case of increasing the noise intensity. $B = 6$; the other model parameters are as in Fig. 18. A jump from a wreath of the curve $x_{2mp}(x_{1mp})$ shown in the figure by a thin dashed line and the arrow corresponds to the disappearance of bimodality.

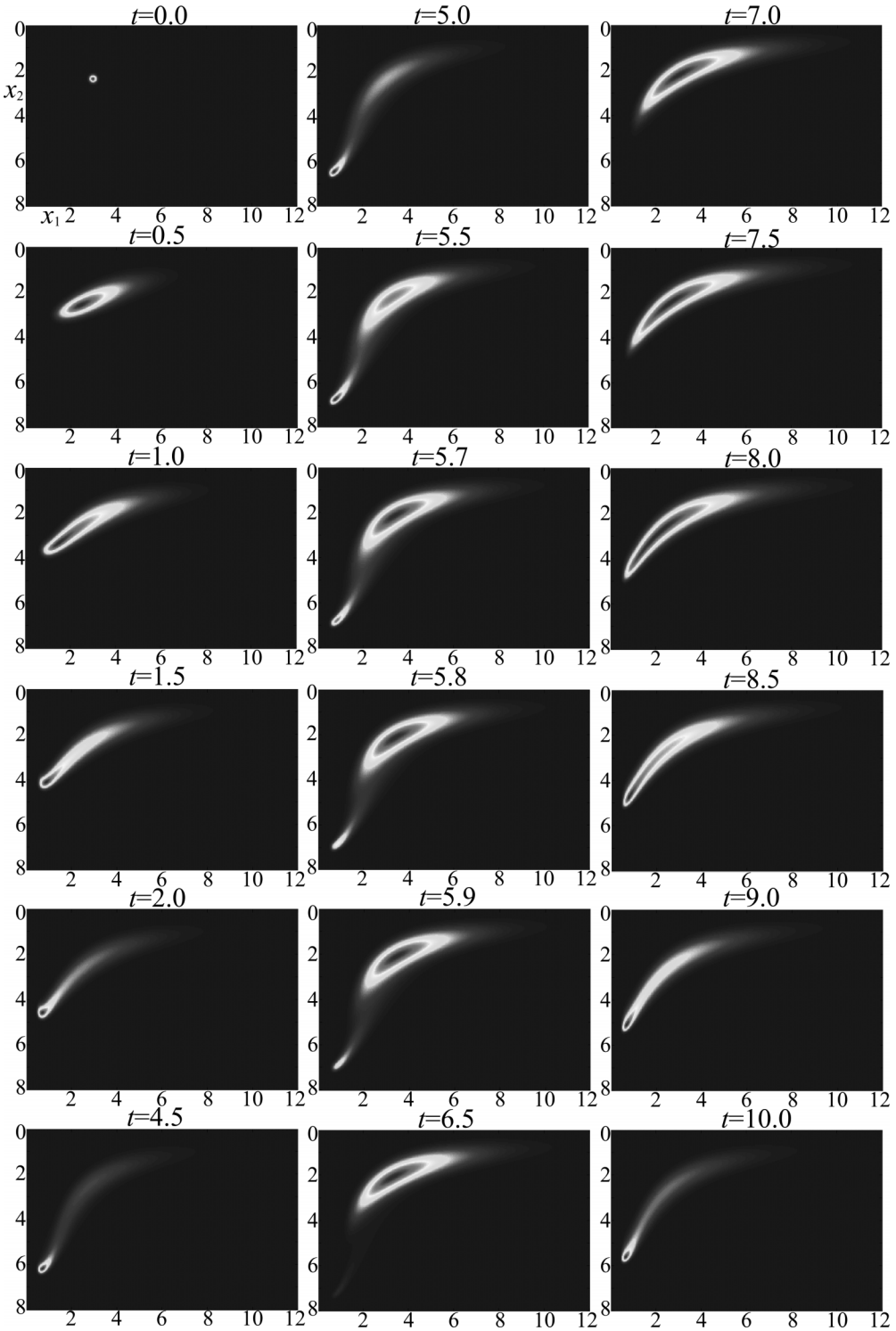

FIG. 21. The evolution of probability density (24) for the model (23). "Repumping" of probability density through bimodality (top view). The model parameters are $B = 7$, $\theta_1 = \theta_2 = \theta = 0.1$. The figure presents one "period" of repumping. The sequences of the frames in the left-hand side and the right-hand side correspond to unimodal distribution, while in the center they correspond to the bimodal one.

probable in the steady stationary state. Figure 16 illustrates this more clearly. All the results given above are quite expectable.

Quite a different picture is observed at a greater distance from the deterministic bifurcation point. Figure 17 presents a more complicated type of the probability density $w(x_1,x_2,t)$ evolution. We can see that at first unimodal distribution is conserved, but it is strongly "blurred" and the maximum of density drifts away from the initial position. Then the splitting of probability density with the formation of two maxima takes place at a certain point in time. Bimodal probability distribution "lives" during a certain time interval. Herewith competition occurs between maxima, as a result of which one

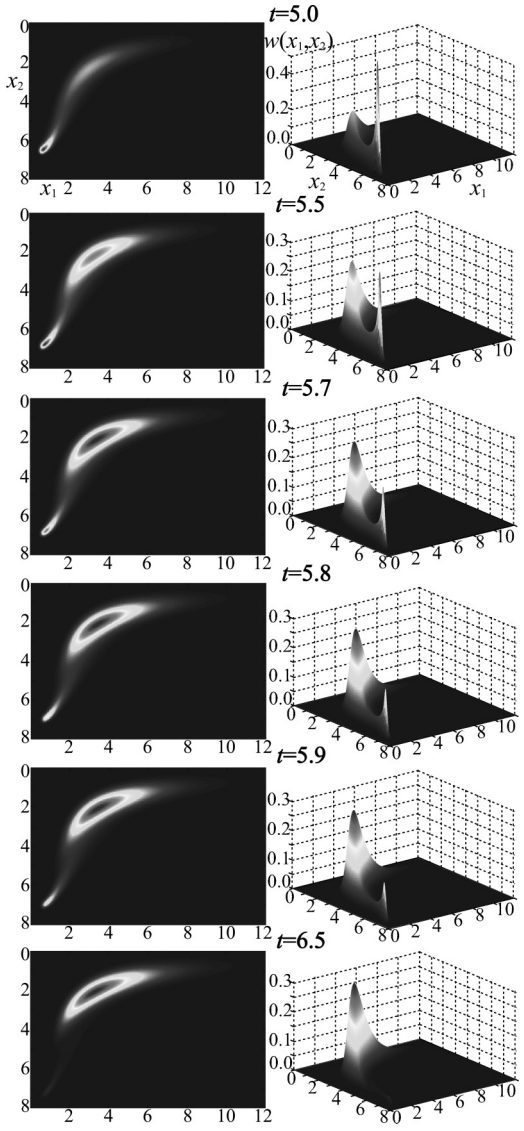

FIG. 22. Repumping of probability density through bimodality (corresponds to the center of Fig. 21).

of the maxima suppresses the other. The distribution becomes unimodal again. That is, transient bimodality is observed in the ordered phase. The behavior of the statistical characteristics also varies as the noise intensity increases.

Figure 18 shows the dependencies of variance Dx_1 of concentration of the first product on time when the noise intensity increases. Figures 19 and 20 demonstrate the appropriate changes of the mean and most probable values. Dependencies $Dx_1(t)$, $Ex_i(t)$,$x_{i\mathrm{mp}}(t)$ are similar to the ones given in Figs. 14, 15, and 16 if the noise intensities θ_1,$\theta_2 < 0.09$. The distribution remains unimodal. A clearly visible "dip" corresponding to the disappearance of transient bimodality is observed in the dependence $Dx_1(t)$ at θ_1,$\theta_2 \geqslant 0.09$. Herewith the discontinuity of the first kind appears in plots of the most probable vs time. The jump from a wreath of the curve $x_{2\mathrm{mp}}(x_{1\mathrm{mp}})$ corresponds to the disappearance of transient bimodality in Fig. 20.

A completely unexpected solution (24) appears at a greater distance from the deterministic point of bifurcation (see Figs. 21–24). At first, density drifts from the initial position to the boundary of the integration region in accordance with the directions indicated in Fig. 12. Then the splitting of density occurs at $t \sim 5$ (Figs. 21 and 22) just as in transient bimodality.

Peculiar "repumping" of probability density from one maximum to another through bimodality is observed until the time moment $t \sim 6.5$ (Fig. 22). It can be noticed that the duration of the existence of one- and bimodal distributions are comparable in the order of magnitude. Then a drift towards the boundaries happens again. The process is repeated until the stationary state is established. This is accompanied by "oscillations" in $Dx_i(t)$ (Fig. 23) and a decrease in the size of the wreath of the curve $Ex_2(Ex_1)$ (Fig. 24). Figure 24 shows two jumps from a wreath of the curve $x_{2\mathrm{mp}}(x_{1\mathrm{mp}})$, which corresponds to the double appearance and disappearance of repumping of the probability density through bimodality.

Such behavior of the probability density implies multiple appearance of the other state (other phase) that corresponds to bimodal distribution in the ordered phase. We can assume that there is a kind of phase "intermittency." This noise-induced effect will be presented in more detail in our future paper.

So, as a result of the numerical study of Eq. (24) solutions we found that different types of solutions can arise in the region of Turing bifurcation when noise intensity increases: unimodal distribution, unimodal distribution with transient bimodality, and complicated distribution, in which unimodal and bimodal distributions alternate until the steady state is established. In other words, only the ordered phase is observed at low noise intensity. The increase of the noise intensity leads to the appearance of transient bimodality (disordered phase) in the ordered phase. Further growth of the noise intensity disrupts the ordering to an even greater extent: There is an intermittency phase, which "swings" the ordered state, as it were.

B. Fokker-Planck equation for order parameters

The system (23) analysis presented above takes into account the interaction of the whole set of both stable and unstable modes. It is known that the system behavior is governed by the behavior of unstable modes (order parameters) [41] in the vicinity of the Turing bifurcation point. Therefore, additionally we study the behavior of order parameters of this system. The procedure of deriving generalized Ginzburg-Landau equations for type (1) systems was proposed in Ref. [27]. Following this procedure we obtained stochastic equations for the amplitudes of unstable modes for system (23). These equations have the

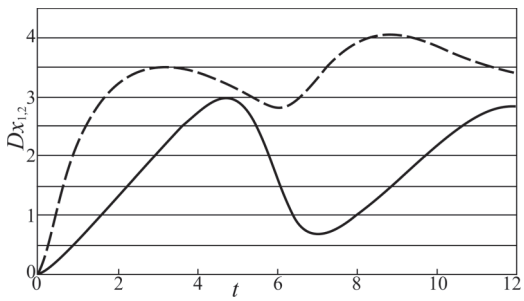

FIG. 23. Dependencies of variances Dx_1 and Dx_2 on time at $B = 7, \theta_1 = \theta_2 = \theta = 0.1$. The figure presents one "period of repumping."

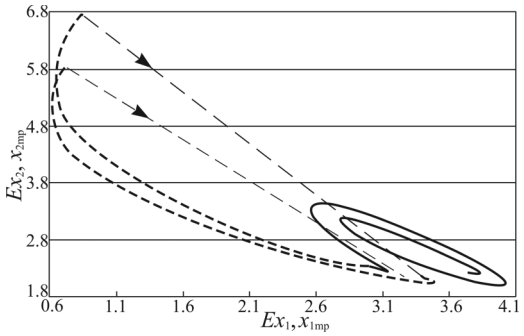

FIG. 24. Change of the mean (solid line) and the most probable (dashed line) values x_1 and x_2 in repumping. Two periods are presented.

form

$$\frac{d\xi^{(1)}_{\mathbf{k}u}}{d\tau} = F_{\mathbf{k}u}(\tau), \tag{25}$$

$$\begin{aligned} F_{\mathbf{k}u}(\tau) &= \lambda_1(\mathbf{k}_u)\xi^{(1)}_{\mathbf{k}u} + \sum_{\mathbf{k}'u} \Omega_1(\mathbf{k}_u,\mathbf{k}'_u,\mathbf{k}_s,\mathbf{z}(\tau))\xi^{(1)}_{\mathbf{k}'u} \\ &+ \sum_{\mathbf{k}'u\mathbf{k}''u} \Omega_{11}(\mathbf{k}_u,\mathbf{k}'_u,\mathbf{k}''_u,\mathbf{k}_s,\mathbf{z}(\tau))\xi^{(1)}_{\mathbf{k}'u}\xi^{(1)}_{\mathbf{k}''u} \\ &+ \sum_{\mathbf{k}'u\mathbf{k}''u\mathbf{k}'''u} \omega(\mathbf{k}_u,\mathbf{k}'_u,\mathbf{k}''_u,\mathbf{k}'''_u)\xi^{(1)}_{\mathbf{k}'u}\xi^{(1)}_{\mathbf{k}''u}\xi^{(1)}_{\mathbf{k}'''u} \\ &+ A\left[-O^{*(1)}_1(\mathbf{k}_u)z_{1,\mathbf{k}u}(\tau) + O^{*(1)}_2(\mathbf{k}_u)z_{2,\mathbf{k}u}(\tau)\right] \\ &- \sum_{\mu,\varphi,\varphi'=1}^{2} \sum_{\mathbf{k}s} \zeta^{(\mu)}_{\varphi\varphi'}(\mathbf{k}_s,\mathbf{k}_u)z_{\varphi',\mathbf{k}u-\mathbf{k}s}(\tau)z_{\varphi,\mathbf{k}s}(\tau). \end{aligned}$$

Here $\xi^{(1)}_{\mathbf{k}u}$ are unstable mode amplitudes of system (23), $\mathbf{k}_u,\mathbf{k}_s$ are wave numbers of unstable and stable modes, respectively, $\mathbf{z}(\tau)$ is the random vector field, the components of which $z_{\varphi,\mathbf{k}}(\tau) = \int \xi_\varphi(\mathbf{r},\tau)e^{-i\mathbf{k}\mathbf{r}}d\mathbf{r}$ have zero means and a given correlation tensor $K[z_{j,\mathbf{k}}(t),z_{l,\mathbf{k}'}(\tau)] = g_{jl}(|\mathbf{k}|)\delta(\mathbf{k}-\mathbf{k}')\delta(t-\tau)\delta_{jl}$, and φ and $\mathbf{k}$ are index arguments of this field.

Taking into account that the functions $\Phi_i(|\mathbf{r}-\mathbf{r}'|)$ in Eqs. (1) were chosen to be exponential for definiteness, for two-dimensional media $g_{ii} = \theta_i k_{fi}/[2\pi^2(k^2+k^2_{fi})^{-3/2}]$. Functions $\lambda_1(\mathbf{k}_u)$, $\Omega_1(\mathbf{k}_u,\mathbf{k}'_u,\mathbf{k}_s,\mathbf{z}(\tau))$, $\Omega_{11}(\mathbf{k}_u,\mathbf{k}'_u,\mathbf{k}''_u,\mathbf{k}_s,\mathbf{z}(\tau))$, and others introduced in Eq. (25) are presented in Appendix B.

Equations (25) define the evolution of a set of random processes. Let us write FPE for these processes. It can be represented in a general form as follows:

$$\begin{aligned} &\frac{\partial w(\{\xi^{(1)}_{\mathbf{k}u}\},\tau)}{\partial\tau} \\ &= -\sum_{\mathbf{k}u}\frac{\partial}{\partial\xi^{(1)}_{\mathbf{k}u}}\left(\left\{\langle F_{\mathbf{k}u}(\tau)\rangle + \sum_{\mathbf{q}u}\int_{-\infty}^{0} K\left[\frac{\partial F_{\mathbf{k}u}(\tau)}{\partial\xi^{(1)}_{\mathbf{q}u}}, F_{\mathbf{q}u}(t')\right]dt'\right\}w\right) \\ &+ \sum_{\mathbf{k}u,\mathbf{q}u}\frac{\partial^2}{\partial\xi^{(1)}_{\mathbf{k}u}\partial\xi^{(1)}_{\mathbf{q}u}}\left(\left\{\int_{-\infty}^{0} K[F_{\mathbf{k}u}(\tau),F_{\mathbf{q}u}(t')]dt'\right\}w\right). \end{aligned} \tag{26}$$

Here $w(\{\xi^{(1)}_{\mathbf{k}u}\},\tau)$ is the multivariate probability distribution density defining the probability of some configuration of unstable modes $\{\xi^{(1)}_{\mathbf{k}u}\}$. After transformations with an accuracy up to the terms linear in the noise intensity one can obtain the correlation functions appearing in Eq. (26) that are presented in Appendix C.

Let the space of the system under study be two-dimensional. If only one mode with the wave number $\mathbf{k}_c$ and amplitude $\xi_{\mathbf{k}c}$ is unstable in such space the Eq. (26) acquires a simple structure:

$$\begin{aligned} \frac{\partial w(\xi_{\mathbf{k}c},\tau)}{\partial\tau} = -\frac{\partial}{\partial\xi_{\mathbf{k}c}}\Big\{&\left(h + a\xi_{\mathbf{k}c} + b\xi^3_{\mathbf{k}c}\right)w \\ &- \left(c + d\xi^2_{\mathbf{k}c} + e\xi^4_{\mathbf{k}c}\right)\frac{\partial w}{\partial\xi_{\mathbf{k}c}}\Big\}. \end{aligned} \tag{27}$$

Constants a, b, c, d, e, and h are easily obtained assuming that $\mathbf{k}'_u = \mathbf{q}'_u = \mathbf{q}''_u = \mathbf{k}_c$ in correlators $K[\frac{\partial F_{\mathbf{k}u}(\tau)}{\partial\xi^{(1)}_{\mathbf{q}u}}, F_{\mathbf{q}u}(t')]$ and $K[F_{\mathbf{k}u}(\tau),F_{\mathbf{q}u}(t')]$ (see Appendix C).

The stationary solution of Eq. (27) has the form

$$w_{st}(\xi_{\mathbf{k}c}) = \begin{cases} N\left|c + d\xi^2_{\mathbf{k}c} + e\xi^4_{\mathbf{k}c}\right|^{\frac{b}{4e}}\left|\frac{2e\xi^2_{\mathbf{k}c}+d-\sqrt{d^2-4ec}}{2e\xi^2_{\mathbf{k}c}+d+\sqrt{d^2-4ec}}\right|^{\frac{2ae-bd}{4e\sqrt{d^2-4ec}}}\exp I, & d^2 > 4ec, \\ N\left|c + d\xi^2_{\mathbf{k}c} + e\xi^4_{\mathbf{k}c}\right|^{\frac{b}{4e}}\exp\left\{\frac{2ae-bd}{2e\sqrt{4ec-d^2}}\arctan\left(\frac{2e\xi^2_{\mathbf{k}c}+d}{\sqrt{4ec-d^2}}\right)\right\}\exp I, & 4ec > d^2. \end{cases} \tag{28}$$

Here

$$I = \begin{cases} \frac{eh}{\sqrt{d^2-4ec}}(I_1 - I_2), & d^2 > 4ec, \\ \frac{h}{4e\sin\alpha}\left[\sin\frac{\alpha}{2}\ln\left(\frac{\xi^2_{\mathbf{k}c}+2q\xi_{\mathbf{k}c}\cos\frac{\alpha}{2}+q^2}{\xi^2_{\mathbf{k}c}-2q\xi_{\mathbf{k}c}\cos\frac{\alpha}{2}+q^2}\right) + 2\cos\frac{\alpha}{2}\arctan\left(\frac{\xi^2_{\mathbf{k}c}-q^2}{2q\xi_{\mathbf{k}c}\sin\frac{\alpha}{2}}\right)\right], & 4ec > d^2; \end{cases}$$

$$\cos\alpha = -d/(2\sqrt{ec}), \quad q = \sqrt[4]{c/e}, \quad f_{1,2} = d/2 \mp (d^2-4ec)^{1/2}/2;$$

$$I_{1,2} = \begin{cases} \frac{1}{\sqrt{ef_{1,2}}}\arctan\left(\xi_{\mathbf{k}c}\sqrt{\frac{e}{f_{1,2}}}\right), & ef_{1,2} > 0, \\ \frac{1}{2i\sqrt{ef_{1,2}}}\ln\left(\frac{f_{1,2}+i\xi_{\mathbf{k}c}\sqrt{ef_{1,2}}}{f_{1,2}-i\xi_{\mathbf{k}c}f_{1,2}}\right), & ef_{1,2} < 0. \end{cases}$$

N is the normalization constant:

$$N = \begin{cases} 1/\int_{-\infty}^{+\infty}\exp I\left|c + d\xi^2_{\mathbf{k}c} + e\xi^4_{\mathbf{k}c}\right|^{\frac{b}{4e}}\left|\frac{2e\xi^2_{\mathbf{k}c}+d-\sqrt{d^2-4ec}}{2e\xi^2_{\mathbf{k}c}+d+\sqrt{d^2-4ec}}\right|^{\frac{2ae-bd}{4e\sqrt{d^2-4ec}}}d\xi_{\mathbf{k}c}, & d^2 > 4ec, \\ 1/\int_{-\infty}^{+\infty}\exp I\left|c + d\xi^2_{\mathbf{k}c} + e\xi^4_{\mathbf{k}c}\right|^{\frac{b}{4e}}\exp\left\{\frac{2ae-bd}{2e\sqrt{4ec-d^2}}\arctan\left(\frac{2e\xi^2_{\mathbf{k}c}+d}{\sqrt{4ec-d^2}}\right)\right\}d\xi_{\mathbf{k}c}, & 4ec > d^2. \end{cases}$$

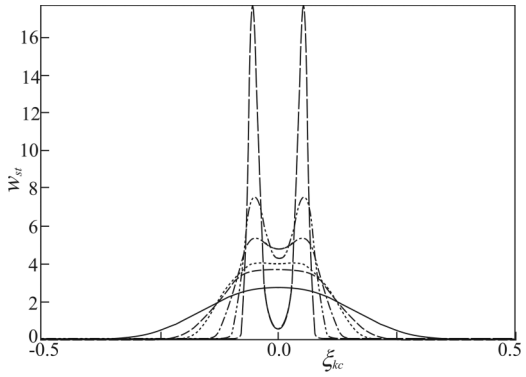

FIG. 25. Steady-state probability density [Eq. (28)] for the values of the critical mode amplitude of system (23) in the supercritical region for six values of noise intensity. $B = 5.5$. Long-dashed line, $\theta_1 = \theta_2 = \theta = 3.5 \times 10^{-5}$; dash-dot-doted line, $\theta = 2.0 \times 10^{-4}$; dash-dotted line, $\theta = 8.0 \times 10^{-4}$; dotted line, $\theta = 3.0 \times 10^{-3}$; dashed line, $\theta = 5.5 \times 10^{-3}$; solid line, $\theta = 2.0 \times 10^{-2}$.

Figure 25 demonstrates the steady-state probability density (28) for the values of the critical mode amplitude of system (23) in the supercritical region for different values of noise intensity. It can be seen from Fig. 25 that two maxima merge into one at $\theta_1 = \theta_2 = 5.5 \times 10^{-3}$ (dashed line) and bimodal distribution is replaced with unimodal. The plot $w_{st}(\xi_{kc})$ acquires a flat top (plateau). Herewith the steady-state most probable value of the critical mode amplitude module $|\xi_{\mathbf{k}c\,\mathrm{mp}}|$ becomes zero (see Fig. 26). It also follows from Fig. 26 that as the distance from the bifurcation point increases, i.e., with the increase of the bifurcation parameter B, the noise intensity, at which $|\xi_{\mathbf{k}c\,\mathrm{mp}}| = 0$, increases. The steady-state mean $\langle|\xi_{\mathbf{k}c}|\rangle$ is always other than zero and the difference between $|\xi_{\mathbf{k}c\,\mathrm{mp}}|$ and $\langle|\xi_{\mathbf{k}c}|\rangle$ increases both with the increase of the noise intensity and that of the parameter B. The latter corresponds to the conclusions from the plots presented in Figs. 16 and 20.

Figure 27 illustrates the behavior of the steady-state second-order cumulant $\kappa_2 = \langle\xi^2_{\mathbf{k}c}\rangle/\langle|\xi_{\mathbf{k}c}|\rangle^2$ and the susceptibility $[\langle\xi^2_{\mathbf{k}c}\rangle - \langle|\xi_{\mathbf{k}c}|\rangle^2]/\theta$ of the order parameter as the noise intensity increases at different values of the bifurcation parameter. The second-order cumulant is a monotone increasing function at low noise, whereas the susceptibility has a marked maximum. This maximum is observed for the values of noise intensity slightly smaller than the values at which $|\xi_{\mathbf{k}c\,\mathrm{mp}}| = 0$. This maximum can be called a "forerunner" of a change in the system state.

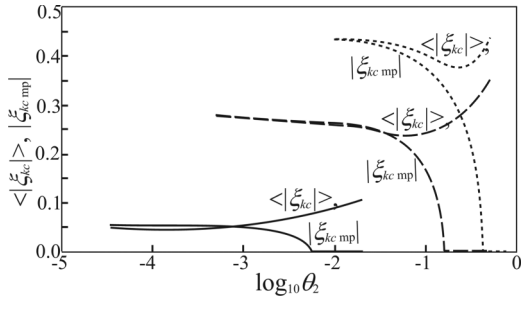

FIG. 26. Steady-state mean $\langle|\xi_{\mathbf{k}c}|\rangle$ and most probable $|\xi_{\mathbf{k}c\,\mathrm{mp}}|$ values of the critical mode amplitude module as a function of noise intensity. Solid line, $B = 5.5$; dashed line, $B = 6.0$; dotted line, $B = 7$.

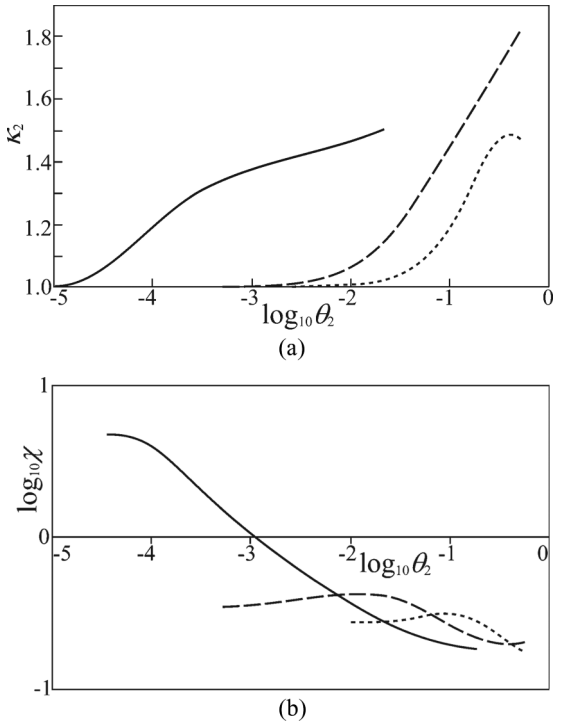

FIG. 27. Steady-state second-order cumulant κ_2 (a) and susceptibility χ (b) as functions of noise intensity. $\theta_2 = \theta_1 = \theta$. Solid line, $B = 5.5$; dashed line, $B = 6.0$; dotted line, $B = 7$.

The analysis of the plots presented in Figs. 14 and 18 shows that the steady-state variance of system (23) increases in the region of low noise. This qualitatively corresponds to the areas where the susceptibility of the order parameter in Fig. 27(b) increases.

One can observe an interesting correspondence between the values of noise intensity at which steady-state bimodal distribution disappears for the critical mode amplitude of system (23) and transient bimodality arises in the ordered phase. We turn to Figs. 19 and 26. At $B = 6$ these values are $\approx$0.16 and $\approx$0.09–0.12, respectively.

V. CONCLUSION

Mean-field approximation was developed for studying the state of multicomponent stochastic spatially extended systems. We assume that in this case equality (10) is true. Herewith the nontrivial spatial structure, spatial homogeneity, and isotropy of multiplicative noise are taken into account. In this approximation a multivariate single-site NSCFPE (12) was derived for the probability density of the state of the system under consideration. The limitations of applying Eq. (12) arise

either due to the limitations of using MFT, which are discussed in [42], or due to the limitations of using Fokker-Planck equation, which are formulated in [34].

The finite-difference method is proposed for the numerical solution of the general class of multivariate nonlinear self-consistent time-dependent Fokker-Planck equations. The accuracy and reliability of the method was illustrated on known one-dimensional problems. It was shown that the method proposed conserves the positive definiteness of solutions and the normalization condition of the probability density unlike the Hermite DAF-based method. In the first order of approximation over time the method proposed makes it possible to obtain solutions with higher accuracy, especially in a steady state and in the region where the solution is close to discontinuity. The necessity of choosing a sufficiently dense uniform grid can be classified as a limitation of the proposed method. However, this can be avoided if the proposed scheme is transferred onto a nonuniform grid. Mean-field approximation was applied to the study of the evolution of the system describing the well-known model of autocatalytic chemical reaction with spatially correlated multiplicative noise. In this paper the region of parameters, in which the Turing bifurcation arises in the deterministic system, was considered.

As a result of the numerical study of NSCFPE solutions for a stochastic spatially extended brusselator we found that only unimodal probability distribution (ordered phase) can be observed at low noise intensity. The increase of noise intensity leads to the occurrence of transient bimodality (disordered phase) in the ordered phase. Further growth of noise intensity disrupts the ordering to an even greater extent: "Intermittency" of unimodal and bimodal distribution, that is "phase intermittency," is observed which "swings" the ordered state. The behavior of variance over time, the most probable and mean of the function defining the system state in case of increasing the external noise intensity and the bifurcation parameter, has been studied. It was shown that the most probable has the discontinuity of the first kind when transient bimodality disappears.

The behavior of the order parameter of the system under consideration was studied. It was shown that some statistical characteristics of the order parameter and the functions defining the system state behave in a similar way in the steady state. Thus, in the vicinity of the bifurcation point the greater the external noise intensity, the greater is the variance in the steady state. Simultaneously the increase of noise intensity leads to the increase of difference between the mean and the appropriate most probable in the steady state. It was shown that transient bimodality occurs in the ordered phase when noise intensity values are close to the values corresponding to the transition from a bimodal density of steady-state order parameter probability distribution to a unimodal one.

ACKNOWLEDGMENTS

The study has been supported by the Ministry of Education and Science of the Russian Federation, Competitiveness Enhancement Program of SSAU and Projects No. 608, No. 102, and No. 1451 of State assignment to educational and research institutions; Grants No. 13-01-970050 r_povolzhie_a, No. 13-01-97001 r_povolzhie_a, and No. 14-02-97030 r_povolzhie_a of the Russian Foundation for Basic Research.

APPENDIX A

A rectangular spatial mesh $\omega_h = (\{ih_1, jh_2\})$ was chosen for problem (24). Here i,j $(i = 0,1,\ldots,I; j = 0,1,\ldots,J)$, h_1,h_2 are indexes of mesh nodes and steps, respectively, and ω_τ is a temporal mesh with a step τ on the interval $0 \leqslant t \leqslant T$. We associate the discrete function w_{ij}^k defined on the mesh $\omega_h \times \omega_\tau$ with the continuous function $w(x_1,x_2,t)$.

We choose the ICs

$$w_0 = w(x_1,x_2,0) = \frac{1}{2\pi\sqrt{\theta_1\theta_2}} \exp\left\{-\frac{(x_1 - x_{10})^2}{2\theta_1} - \frac{(x_2 - x_{20})^2}{2\theta_2}\right\},$$
$$x_{10} = A, \quad x_{20} = B/A$$

and boundary conditions $w(x_1,x_2,t) \to 0$ if $x_1 \to \infty$, $x_2 \to \infty$.

A locally one-dimensional scheme (13)–(15) for problem (24) has the form

$$\frac{w^{k+\alpha/n} - w^{k+(\alpha-1)/n}}{\tau} - \Lambda_\alpha w = 0, \quad w^0 = w_0, \quad \alpha = 1,2; \quad n = 2.$$

$$\Lambda_\alpha w = [a_\alpha (q_\alpha w)_{\bar{x}_\alpha}]_{x_\alpha},$$

$$q_1 = \exp\left(\frac{a_0}{x_1} + a_1 \ln|x_1| - \frac{x_1x_2}{\theta_1}\right),$$

$$q_2 = \exp\left[-b_1(x_1)x_2 + b_2(x_1)x_2^2\right],$$

$$a_{1,i} = \left\{\frac{1}{2\theta_1}\left[\exp\left(\frac{a_0}{x_{1,i}} - \frac{x_{1,i}x_2}{\theta_1}\right)x_{1,i}^{a_1-2} + \exp\left(\frac{a_0}{x_{1,i-1}} - \frac{x_{1,i-1}x_2}{\theta_1}\right)x_{1,i-1}^{a_1-2}\right]\right\}^{-1}, \quad x_{1,i} = ih_1,$$

$$a_{2,j} = \left(\frac{1}{2\theta_2 x_1^2}\left\{\exp\left[-b_1(x_1)x_{2,j} + b_2(x_1)x_{2,j}^2\right] + \exp\left[-b_1(x_1)x_{2,j-1} + b_2(x_1)x_{2,j-1}^2\right]\right\}\right)^{-1},$$

$$x_{2,j} = jh_2.$$

Here the notations are introduced:

$$a_0 = \frac{A + D_1E(x_1|x_2,t)}{\theta_1}, \quad a_1 = \frac{B + 1 + \theta_1 + D_1}{\theta_1},$$
$$b_1(x_1) = \frac{B}{\theta_2 x_1} + \frac{D_2E(x_2|x_1,t)}{\theta_2 x_1^2}, \quad b_2(x_1) = \frac{x_1^2 + D_2}{2\theta_2 x_1^2}.$$

On the boundary,

$$w^k_{1j} = w^k_{0j} \sim 0, \quad w^k_{i1} = w^k_{i0} \sim 0, \quad w^k_{Ij} = w^k_{I-1j} \sim 0, \quad w^k_{iJ} = w^k_{iJ-1} \sim 0.$$

At the transition to a semilayer,

$$-B_i w^{k+1/2}_{i+1j} + C_i w^{k+1/2}_{ij} - A_i w^{k+1/2}_{i-1j} = w^k_{ij};$$

$$A_0 = 0; \quad B_0 = 1; \quad C_0 = 1; \quad F_0 = 0; \quad A_I = 1; \quad B_I = 0; \quad C_I = 1; \quad F_I = 0;$$

$$A_i = \frac{\tau\theta_1}{h_1^2} \frac{|x_1 - h_1|^2}{1 + \exp\left\{-\frac{a_0 h_1}{x_1(x_1-h_1)} - \frac{x_2 h_1}{\theta_1} + (a_1 - 2)\ln\left|\frac{x_1}{x_1-h_1}\right|\right\}},$$

$$B_i = \frac{\tau\theta_1}{h_1^2} \frac{|x_1 + h_1|^2}{1 + \exp\left\{\frac{a_0 h_1}{x_1(x_1+h_1)} + \frac{x_2 h_1}{\theta_1} + (a_1 - 2)\ln\left|\frac{x_1}{x_1+h_1}\right|\right\}},$$

$$C_i = 1 + \frac{\tau\theta_1 x_1^2}{h_1^2} \frac{1}{1 + \exp\left\{-\frac{a_0 h_1}{x_1(x_1+h_1)} - \frac{x_2 h_1}{\theta_1} + (a_1 - 2)\ln\left|\frac{x_1+h_1}{x_1}\right|\right\}} + \frac{\tau\theta_1 x_1^2}{h_1^2} \frac{1}{1 + \exp\left\{\frac{a_0 h_1}{x_1(x_1-h_1)} + \frac{x_2 h_1}{\theta_1} + (a_1 - 2)\ln\left|\frac{x_1-h_1}{x_1}\right|\right\}}.$$

At the transition to a whole layer,

$$-B_j w^{k+1}_{ij+1} + C_j w^{k+1}_{ij} - A_j w^{k+1}_{ij-1} = w^{k+1/2}_{ij};$$

$$A_0 = 0; \quad B_0 = 1; \quad C_0 = 1; \quad F_0 = 0; \quad A_J = 1; \quad B_J = 0; \quad C_J = 1; \quad F_J = 0;$$

$$A_j = \frac{\tau\theta_2 x_1^2}{h_2^2} \frac{1}{1 + \exp\{-b_1 h_2 + 2b_2 h_2 (x_2 - 0.5h_2)\}},$$

$$B_j = \frac{\tau\theta_2 x_1^2}{h_2^2} \frac{1}{1 + \exp\{b_1 h_2 - 2b_2 h_2 (x_2 + 0.5h_2)\}},$$

$$C_j = 1 + \frac{\tau\theta_2 x_1^2}{h_1^2}\left[\frac{1}{1 + \exp\{-b_1 h_2 + 2b_2 h_2 (x_2 + 0.5h_2)\}} + \frac{1}{1 + \exp\{b_1 h_2 - 2b_2 h_2 (x_2 - 0.5h_2)\}}\right].$$

APPENDIX B

The functions introduced in Eq. (25) can be written as follows:

$$\lambda_\mu(\mathbf{k}) = \frac{\alpha(\mathbf{k})}{2} \pm \sqrt{\frac{\alpha^2(\mathbf{k})}{4} - \beta(\mathbf{k})},$$

$$\alpha(\mathbf{k}) = B - 1 - A^2 - (D_1 + D_2)k^2, \quad \beta(\mathbf{k}) = [A^2 D_1 - (B-1)D_2]k^2 + D_1 D_2 k^4 + A^2,$$

$$\Omega_1(\mathbf{k}_u, \mathbf{k}'_u, \mathbf{k}_s, \mathbf{z}(\tau)) = \sum_{\mu,\varphi} \eta^{(\mu)}_\varphi(\mathbf{k}_u, \mathbf{k}'_u) z_{\varphi, \mathbf{k}u - \mathbf{k}'u} - \sum_{\mathbf{k}'s} \sum_{\mu,\varphi,\varphi'} A^{(\mu)}_{\varphi\varphi'}(\mathbf{k}'_u, \mathbf{k}_s, \mathbf{k}_u) z_{\varphi, \mathbf{k}u - \mathbf{k}s} z_{\varphi', \mathbf{k}s - \mathbf{k}'u},$$

$$\Omega_{11}(\mathbf{k}_u, \mathbf{k}'_u, \mathbf{k}''_u, \mathbf{k}_s, \mathbf{z}(\tau)) = \delta(\mathbf{k}_u, \mathbf{k}'_u, \mathbf{k}''_u) - \sum_{\mu,\varphi} (-1)^\varphi \nu^{(\mu)}_\varphi(\mathbf{k}_u, \mathbf{k}'_u, \mathbf{k}''_u) z_{\varphi, \mathbf{k}u - \mathbf{k}'u - \mathbf{k}''u},$$

$$\eta^{(\mu)}_\varphi(\mathbf{k}_u, \mathbf{k}'_u) = (-1)^\varphi \left[O^{(1)}_1(\mathbf{k}'_u) O^{*(1)}_\varphi(\mathbf{k}_u) - \beta^{(\mu)}_\varphi(\mathbf{k}_u, \mathbf{k}'_u)\right],$$

$$A^{(\mu)}_{\varphi\varphi'}(\mathbf{k}'_u, \mathbf{k}_s, \mathbf{k}_u) = (-1)^{\varphi+\varphi'} O^{(1)}_1(\mathbf{k}'_u) \varepsilon^{(\mu)}_{\varphi\varphi'}(\mathbf{k}_s, \mathbf{k}'_u),$$

$$\zeta^{(\mu)}_{\varphi\varphi'}(\mathbf{k}_s, \mathbf{k}_u) = (-1)^{\varphi+\varphi'} A \varepsilon^{(\mu)}_{\varphi\varphi'}(\mathbf{k}_s, \mathbf{k}'_u),$$

$$\varepsilon^{(\mu)}_{\varphi\varphi'}(\mathbf{k}_s, \mathbf{k}'_u) = \frac{O^{(\mu)}_1(\mathbf{k}_s)}{\lambda_\mu(\mathbf{k}_s)} O^{*(\mu)}_\varphi(\mathbf{k}_s) O^{*(1)}_{\varphi'}(\mathbf{k}_u),$$

$$\beta^{(\mu)}_\varphi(\mathbf{k}_u, \mathbf{k}'_u) = \frac{O^{*(1)}_1(\mathbf{k}_u) - O^{*(1)}_2(\mathbf{k}_u)}{\lambda_\mu(|\mathbf{k}_u - \mathbf{k}'_u|)} O^{*(\mu)}_\varphi(|\mathbf{k}_u - \mathbf{k}'_u|) \sigma^{1\mu}(\mathbf{k}_u, |\mathbf{k}_u - \mathbf{k}'_u|),$$

$$\nu^{(\mu)}_\varphi(\mathbf{k}_u, \mathbf{k}'_u, \mathbf{k}''_u) = \beta^{(\mu)}_\varphi(\mathbf{k}_u, \mathbf{k}'_u) O^{(1)}_1(\mathbf{k}''_u) + O^{*(1)}_\varphi(\mathbf{k}_u) \frac{O^{(\mu)}_1(|\mathbf{k}'_u + \mathbf{k}''|_u)}{\lambda_\mu(|\mathbf{k}'_u + \mathbf{k}''_u|)} \left[O^{*(\mu)}_1(|\mathbf{k}'_u + \mathbf{k}''_u|) - O^{*(\mu)}_2(|\mathbf{k}'_u + \mathbf{k}''_u|)\right] \left[2A O^{(1)}_1(\mathbf{k}'_u) O^{(1)}_2(\mathbf{k}''_u) + \frac{B}{A} O^{(1)}_1(\mathbf{k}'_u) O^{(1)}_1(\mathbf{k}''_u)\right],$$

$$\delta(\mathbf{k}_u,\mathbf{k}'_u,\mathbf{k}''_u) = \left[O_1^{*(1)}(\mathbf{k}_u) - O_2^{*(1)}(\mathbf{k}_u)\right]\left[2AO_1^{(1)}(\mathbf{k}'_u)O_2^{(1)}(\mathbf{k}''_u) + \frac{B}{A}O_1^{(1)}(\mathbf{k}'_u)O_1^{(1)}(\mathbf{k}''_u)\right]\delta(\mathbf{k}_u - \mathbf{k}'_u - \mathbf{k}''_u),$$

$$\begin{aligned}\omega(\mathbf{k}_u,\mathbf{k}'_u,\mathbf{k}''_u,\mathbf{k}'''_u) &= \left[O_1^{*(1)}(\mathbf{k}_u) - O_2^{*(1)}(\mathbf{k}_u)\right]O_1^{(1)}(\mathbf{k}'_u)O_1^{(1)}(\mathbf{k}''_u)O_2^{(1)}(\mathbf{k}'''_u)\delta(\mathbf{k}_u - \mathbf{k}'_u - \mathbf{k}''_u - \mathbf{k}'''_u)\\ &- \sum_{\mathbf{k}s,\mu}\left\{\frac{\left[O_1^{*(1)}(\mathbf{k}_u) - O_2^{*(1)}(\mathbf{k}_u)\right]}{\lambda_\mu(\mathbf{k}_s)}\sigma^{1\mu}(\mathbf{k}'_u,\mathbf{k}_s)\left[O_1^{*(\mu)}(\mathbf{k}_s) - O_2^{*(\mu)}(\mathbf{k}_s)\right]\right.\\ &\left.\times\left[2AO_1^{(1)}(\mathbf{k}'''_u)O_2^{(1)}(\mathbf{k}''_u) + \frac{B}{A}O_1^{(1)}(\mathbf{k}'''_u)O_1^{(1)}(\mathbf{k}''_u)\right]\delta(\mathbf{k}_u - \mathbf{k}'_u - \mathbf{k}_s)\delta(\mathbf{k}_s - \mathbf{k}''_u - \mathbf{k}'''_u)\right\},\end{aligned}$$

$$\sigma^{1\mu}(\mathbf{k}'_u,\mathbf{k}_s) = 2AO_1^{(1)}(\mathbf{k}'_u)O_2^{(\mu)}(\mathbf{k}_s) + 2\frac{B}{A}O_1^{(1)}(\mathbf{k}'_u)O_1^{(\mu)}(\mathbf{k}_s) + 2AO_1^{(\mu)}(\mathbf{k}_s)O_2^{(1)}(\mathbf{k}'_u),$$

$$\mathbf{O}^{(\mu)}(\mathbf{k}) = \begin{pmatrix}[-A^2 - D_2k^2 - \lambda_\mu(\mathbf{k})]/B\\ 1\end{pmatrix},$$

$$\mathbf{O}^{*(\mu)}(\mathbf{k}) = \begin{pmatrix}(-1)^\mu O_2^{(\mu')}(\mathbf{k})/\left[O_2^{(1)}(\mathbf{k})O_1^{(2)}(\mathbf{k}) - O_2^{(2)}(\mathbf{k})O_1^{(1)}(\mathbf{k})\right]\\ (-1)^{\mu'} O_1^{(\mu')}(\mathbf{k})/\left[O_2^{(1)}(\mathbf{k})O_1^{(2)}(\mathbf{k}) - O_2^{(1)}(\mathbf{k})O_1^{(1)}(\mathbf{k})\right]\end{pmatrix}, \quad \text{if } \mu = 1, \quad \mu' = 2; \quad \text{if } \mu = 2, \quad \mu' = 1.$$

APPENDIX C

The correlators from Eq. (26) can be written as follows:

$$\begin{aligned}K\left[\frac{\partial F_{\mathbf{k}u}(\tau)}{\partial\xi^{(1)}_{\mathbf{q}u}}, F_{\mathbf{q}u}(t')\right] &= \sum_\varphi \eta_\varphi(\mathbf{k}_u,\mathbf{q}_u)O_\varphi^{*(1)}(\mathbf{q}_u)p_\varphi^{(0)}g_{\varphi\varphi}(|\mathbf{k}_u - \mathbf{q}_u|)\delta_{\mathbf{k}u-\mathbf{q}u,qu}\delta(\tau - t')\\ &+ \sum_\varphi [\nu_\varphi(\mathbf{k}_u,\mathbf{q}_u,\mathbf{k}_u - 2\mathbf{q}_u) + \nu_\varphi(\mathbf{k}_u,\mathbf{k}_u - 2\mathbf{q}_u,\mathbf{q}_u)]O_\varphi^{*(1)}(\mathbf{q}_u)p_\varphi^{(0)}g_{\varphi\varphi}(|\mathbf{q}_u|)\xi_{\mathbf{k}u-2\mathbf{q}u}\delta(\tau - t')\\ &+ \sum_\varphi \eta_\varphi(\mathbf{k}_u,\mathbf{q}_u)\eta_\varphi(\mathbf{q}_u,2\mathbf{q}_u - \mathbf{k}_u)g_{\varphi\varphi}(|\mathbf{k}_u - \mathbf{q}_u|)\xi_{2\mathbf{q}u-\mathbf{k}u}\delta(\tau - t')\\ &+ \sum_{\varphi,\mathbf{q}'u} \eta_\varphi(\mathbf{k}_u,\mathbf{q}_u)\nu_\varphi(\mathbf{q}_u,\mathbf{q}'_u,2\mathbf{q}_u - \mathbf{k}_u - \mathbf{q}'_u)g_{\varphi\varphi}(|\mathbf{k}_u - \mathbf{q}_u|)\xi_{\mathbf{q}'u}\xi_{2\mathbf{q}u-\mathbf{k}u-\mathbf{q}'u}\delta(\tau - t')\\ &+ \sum_{\varphi,\mathbf{q}'u,\mathbf{q}''u} [\nu_\varphi(\mathbf{k}_u,\mathbf{q}_u,\mathbf{k}_u - 2\mathbf{q}_u + \mathbf{q}'_u + \mathbf{q}''_u) + \nu_\varphi(\mathbf{k}_u,\mathbf{k}_u - 2\mathbf{q}_u + \mathbf{q}'_u + \mathbf{q}''_u,\mathbf{q}_u)]\\ &\times \nu_\varphi(\mathbf{q}_u,\mathbf{q}'_u,\mathbf{q}''_u)g_{\varphi\varphi}(|\mathbf{q}_u - \mathbf{q}'_u - \mathbf{q}''_u|)\xi_{\mathbf{q}'u}\xi_{\mathbf{q}''u}\xi_{\mathbf{k}u-2\mathbf{q}u+\mathbf{q}'u+\mathbf{q}''u}\delta(\tau - t')\\ &+ \sum_{\varphi,\mathbf{q}'u} \eta_\varphi(\mathbf{q}_u,\mathbf{q}'_u)[\nu_\varphi(\mathbf{k}_u,\mathbf{k}_u - 2\mathbf{q}_u + \mathbf{q}'_u,\mathbf{q}_u) + \nu_\varphi(\mathbf{k}_u,\mathbf{q}_u,\mathbf{k}_u - 2\mathbf{q}_u + \mathbf{q}'_u)]\\ &\times g_{\varphi\varphi}(|\mathbf{q}_u - \mathbf{q}'_u|)\xi_{\mathbf{q}'u}\xi_{\mathbf{k}u-2\mathbf{q}u+\mathbf{q}'u}\delta(\tau - t'),\end{aligned}$$

$$\begin{aligned}K[F_{\mathbf{k}u}(\tau), F_{\mathbf{q}u}(t')] &= \sum_\varphi \left[O_\varphi^{*(1)}(\mathbf{k}_u)\right]^2\left(p_\varphi^{(0)}\right)^2 g_{\varphi\varphi}(|\mathbf{k}_u|)\delta_{\mathbf{k}u,\mathbf{q}u}\delta(\tau - t')\\ &+ \sum_\varphi \eta_\varphi(\mathbf{k}_u,\mathbf{k}_u - \mathbf{q}_u)O_\varphi^{*(1)}(\mathbf{q}_u)p_\varphi^{(0)}g_{\varphi\varphi}(|\mathbf{q}_u|)\xi_{\mathbf{k}u-\mathbf{q}u}\delta(\tau - t')\\ &+ \sum_\varphi \eta_\varphi(\mathbf{q}_u,\mathbf{q}_u - \mathbf{k}_u)O_\varphi^{*(1)}(\mathbf{k}_u)p_\varphi^{(0)}g_{\varphi\varphi}(|\mathbf{k}_u|)\xi_{\mathbf{q}u-\mathbf{k}u}\delta(\tau - t')\\ &+ \sum_{\varphi,\mathbf{q}'u} \eta_\varphi(\mathbf{k}_u,\mathbf{k}_u - \mathbf{q}_u + \mathbf{q}'_u)\eta_\varphi(\mathbf{q}_u,\mathbf{q}'_u)g_{\varphi\varphi}(|\mathbf{q}_u - \mathbf{q}'_u|)\xi_{\mathbf{q}'u}\xi_{\mathbf{k}u-\mathbf{q}u+\mathbf{q}'u}\delta(\tau - t')\\ &+ \sum_{\varphi,\mathbf{k}'u,\mathbf{q}'u} \nu_\varphi(\mathbf{k}_u,\mathbf{k}'_u,\mathbf{k}_u - \mathbf{k}'_u - \mathbf{q}_u + \mathbf{q}'_u)\eta_\varphi(\mathbf{q}_u,\mathbf{q}'_u)g_{\varphi\varphi}(|\mathbf{q}_u - \mathbf{q}'_u|)\xi_{\mathbf{k}'u}\xi_{\mathbf{q}'u}\xi_{\mathbf{k}u-\mathbf{k}'u-\mathbf{q}u+\mathbf{q}'u}\delta(\tau - t')\\ &+ \sum_{\varphi,\mathbf{q}'u} \nu_\varphi(\mathbf{q}_u,\mathbf{q}'_u,\mathbf{q}_u - \mathbf{q}'_u - \mathbf{k}_u)O_\varphi^{*(1)}(\mathbf{k}_u)p_\varphi^{(0)}g_{\varphi\varphi}(|\mathbf{k}_u|)\xi_{\mathbf{q}'u}\xi_{\mathbf{q}u-\mathbf{q}'u-\mathbf{k}u}\delta(\tau - t')\end{aligned}$$

$$+\sum_{\varphi,\mathbf{k}'u,\mathbf{q}'u}\nu_\varphi(\mathbf{q}_u,\mathbf{q}'_u,\mathbf{q}_u-\mathbf{q}'_u-\mathbf{k}_u+\mathbf{k}'_u)\eta_\varphi(\mathbf{k}_u,\mathbf{k}'_u)g_{\varphi\varphi}(|\mathbf{k}_u-\mathbf{k}'_u|)\xi_{\mathbf{k}'u}\xi_{\mathbf{q}'u}\xi_{\mathbf{q}u-\mathbf{q}'u-\mathbf{k}u+\mathbf{k}'u}\delta(\tau-t')$$

$$+\sum_{\varphi,\mathbf{k}'u,\mathbf{q}'u,\mathbf{q}''u}\nu_\varphi(\mathbf{k}_u,\mathbf{k}'_u,\mathbf{k}_u-\mathbf{k}'_u-\mathbf{q}_u+\mathbf{q}'_u+\mathbf{q}''_u)\nu_\varphi(\mathbf{q}_u,\mathbf{q}'_u,\mathbf{q}''_u)$$

$$\times g_{\varphi\varphi}(|\mathbf{q}_u-\mathbf{q}'_u-\mathbf{q}''_u|)\xi_{\mathbf{k}'u}\xi_{\mathbf{q}'u}\xi_{\mathbf{q}''u}\xi_{\mathbf{k}u-\mathbf{k}'u-\mathbf{q}u+\mathbf{q}'u+\mathbf{q}''u}\delta(\tau-t').$$

[1] B. Lindnera, J. García-Ojalvo, A. Neimand, and L. Schimansky-Geier, Phys. Rep. **392**, 321 (2004).
[2] M. Ibañes, J. García-Ojalvo, R. Toral, and J. M. Sancho, Phys. Rev. E **60**, 3597 (1999).
[3] J. Buceta, M. Ibañes, J. M. Sancho, and K. Lindenberg, Phys. Rev. E **67**, 021113 (2003).
[4] O. Carrillo, M. Ibañes, J. García-Ojalvo, J. Casademunt, and J. M. Sancho, Phys. Rev. E **67**, 046110 (2003).
[5] A. A. Zaikin, J. García-Ojalvo, and L. Schimansky-Geier, Phys. Rev. E **60**, R6275 (1999).
[6] R. Müller, K. Lippert, A. Kühnel, and U. Behn, Phys. Rev. E **56**, 2658 (1997).
[7] O. Carrillo, M. Ibañes, and J. M. Sancho, Fluctuation Noise Lett. **2**, L1 (2002).
[8] P. S. Landa, A. A. Zaikin, L. Schimansky-Geier, Chaos, Solitons Fractals **9**, 1367 (1998).
[9] C. Van den Broeck, J. M. R. Parrondo, R. Toral, and R. Kawai, Phys. Rev. E **55**, 4084 (1997).
[10] J. Buceta, J. M. R. Parrondo, and F. J. de la Rubia, Phys. Rev. E **63**, 031103 (2001).
[11] D. S. Zhang, G. W. Wei, D. J. Kouri, and D. K. Hoffman, Phys. Rev. E **56**, 1197 (1997).
[12] D. S. Zhang, G. W. Wei, D. J. Kouri, and D. K. Hoffman, J. Chem. Phys. **106**, 5216 (1997).
[13] A. N. Drozdov and M. Morillo, Phys. Rev. E **54**, 931 (1996).
[14] H. Chen, J. Duan, and Ch. Zhang, Acta Math. Sci. **32**, 1391 (2012).
[15] P. Kumar and S. Narayanan, Sadhana **31**, 445 (2006).
[16] F. Campillo, M. Joannides, and I. Larramendy-Valverde, Math. Comput. Simul. **99**, 37 (2014).
[17] G. W. Wei, J. Chem. Phys. **110**, 8930 (1999); J. Phys. A: Math. Gen. **33**, 4935 (2000).
[18] D. L. Otten and P. Vedula, J. Stat. Mech. (2011) P09031.
[19] R. O. Fox and P. Vedula, Ind. Eng. Chem. Res. **49**, 5174 (2010).
[20] Y. Kawamura, Phys. Rev. E **76**, 047201 (2007).
[21] M. F. Wehner and W. G. Wolfer, Phys. Rev. A **35**, 1795 (1987).
[22] H. Haken, Z. Phys. B **24**, 321 (1976).
[23] N. G. van Kampen, J. Stat. Phys. **17**, 71 (1977).
[24] H. Tomita, A. Ito, and H. Kidachi, Prog. Theor. Phys. **56**, 786 (1976).
[25] D. Moroni, B. Rotenberg, J.-P. Hansen, S. Succi, and S. Melchionna, Phys. Rev. E **73**, 066707 (2006).
[26] D. L. Ermak and H. Buckholtz, J. Comput. Phys. **35**, 169 (1980).
[27] S. E. Kurushina, V. V. Maximov, and Yu. M. Romanovskii, Phys. Rev. E **86**, 011124 (2012).
[28] I. Prigogine and R. Lefever, J. Chem. Phys. **48**, 1695 (1968).
[29] H. Shimizu and T. Yamada, Prog. Theor. Phys. **47**, 350 (1972).
[30] H. Shimizu, Prog. Theor. Phys. **52**, 329 (1974).
[31] R. C. Desai and R. Zwanzig, J. Stat. Phys. **19**, 1 (1978).
[32] W. Horsthemke and M. Lefever, *Noise-Induced Transition* (Springer, Berlin, 1984).
[33] J. García-Ojalvo, A. M. Lacasta, J. M. Sancho, and R. Toral, Europhys. Lett. **42**, 125 (1998).
[34] R. L. Stratonovich, *Topics in the Theory of Random Noise* (Gordon & Breach, New York, London, 1963), Vol. 1; (Gordon and Breach, New York, London, 1967), Vol. 2.
[35] A. A. Samarskii, USSR Comput. Math. Math. Phys. **2**, 23 (1963).
[36] N. V. Karetkina, USSR Comput. Math. Math. Phys. **20**, 257 (1980).
[37] A. A. Samarskii, USSR Comput. Math. Math. Phys. **2**, 894 (1963).
[38] K. Kometani and H. Shimizu, J. Stat. Phys. **13**, 473 (1975).
[39] A. A. Samarskii, USSR Comput. Math. Math. Phys. **3**, 572 (1963).
[40] A. A. Samarskii, USSR Comput. Math. Math. Phys. **3**, 351 (1963).
[41] H. Haken, *Synergetics* (Springer, Berlin, 2004).
[42] C. Van den Broeck, J. M. R. Parrondo, and R. Toral, Phys. Rev. Lett. **73**, 3395 (1994).